INVESTIGATION OF CLINOPTILOLITE ZEOLITE AS A CANDIDATE SYSTEM FOR STUDY BY POSITRON ANNIHILATION

by

EDWARD PEREZ

Presented to the Faculty of the Graduate School of

The University of Texas at Arlington

In Partial Fulfillment of the Requirements for the Degree of

MASTER OF SCIENCE

THE UNIVERSITY OF TEXAS AT ARLINGTON

December 2020

INVESTIGATION OF CLINOPTILOLITE ZEOLITE AS A CANDIDATE SYSTEM FOR STUDY BY POSITRON ANNIHILATION

The members of the committee who approve the master's thesis of Edward Perez

Alex H. Weiss, Ph.D.
Supervising Professor and
Department Chair of the
Department of Physics _____

Ali R. Koymen, Ph.D.
Head of the Graduate Studies
Committee for the
Department of Physics _____

Qiming Zhang, Ph.D.
Graduate Academic Advisor for the
Department of Physics _____

James Grover, Ph.D.
Associate Dean for Research and
Graduate Studies for
the School of Science _____

To Annie, whom I miss and love very much…

To my mother, who has always loved me unconditionally…

ACKNOWLEDGEMENTS

I would like to sincerely express my deepest gratitude and appreciation to my research and thesis advisor, Dr. Alex H. Weiss; a one of a kind, caring, and warmhearted person. I have been blessed and inspired by his impassioned pursuit of scientific research and his devotion to teaching the younger generations.

I like to express my deepest gratitude to Dr. Ali R. Koymen, Dr. Qiming Zhang, and Dr. Muhammad N. Huda. These researchers have also played the roles of professors, academic advisors, guidance counselors, and, most of all, friends in my life. Their guidance and understanding was essential throughout both my undergraduate and graduate years at this school. Their advice, encouragement, insights, and suggestions have broaden my thinking in both my studies and life.

I am also indebted to the people in my research group. Alexander Jarrett Fairchild and Dr. Randall W. Gladen, have been invaluable throughout the years as they have answered numerous questions on the anti-matter beams and the nature of positrons. Doctoral research candidate Sima Lotfimarangloo was equally as valuable as she more than willing to share her knowledge on the clinoptilolite zeolite and assisted with some of the sample preparation research. Postdoctoral research fellow Dr. Varghese Anto Chirayath is a walking encyclopedia in anything regarding physics or research; I would not have been able to defend my thesis as well as I did if not for his knowledge and guidance. I am thankful for his patience as I know I can be hardheaded and stubborn.

Another person who was not in our research group but assisted with information on zeolite sample preparation is Dr. Jeotikanta Mohapatra. He frequently uses the same instrumentation our research group used to complete this characterization and has deeper insights into sample preparation. His willingness to share his knowledge is a model for all physicist to try to emulate.

I would also like to thank the personnel at the Characterization Center for Materials and Biology (CCMB) at UT Arlington. Mr. Dajing "David" Yan is the Scientific Apparatus Engineering Technician for the scanning electron microscopes and his dedication to his work is invaluable to the CCMB. The high resolution transmission electron microscope instruction

is left for Mr. Yi Shen, another Scientific Apparatus Engineering Technician. Without the information he provided, the completion of this thesis would not be possible. Dr. Jiechao Jiang is the Facility Manager at the CCMB and a Research Faculty in Materials Science and Engineering Department. I have had many informative conversations with Dr. Jiang in which I learned much more information than what I needed to know to complete my project; I highly value and appreciate all the information he has given me.

I also want to thank our department's wonderful administrative assistants: Stacey Nicole Cody, Holly R. Zander, and now retired Angelita Winter. Their patience, devotion, and dedication toward their jobs and our department is both endless and unwavering. They truly are what drives this department forward.

Last but not least, I would like to express my sincerest gratitude to my friends and family. Without their love and support, my journey through undergraduate and graduate education would not have been possible. My deepest apologies for being noticeably absent during what has been almost a decade long educational endeavor.

ABSTRACT

INVESTIGATION OF CLINOPTILOLITE ZEOLITE AS A CANDIDATE SYSTEM FOR STUDY BY POSITRON ANNIHILATION

Publication Number: _____

Edward Perez, MS

The University of Texas at Arlington, 2019

Supervising Professor: Alexander H. Weiss

This thesis reports on the characterization of a clinoptilolite zeolite ($Na_3[Al_3Si_{15}O_{36}]12H_2O$) using Energy-dispersive X-ray spectroscopy (EDX/EDS) for chemical analysis, low energy Secondary Electron (SE) analysis for three-dimensional imaging and topography, and Transmission Electron Microscopy (TEM) for two-dimensional imaging at the nanometer level. The goal of this work was to provide additional information that can aid in the interpretation of the data obtained using positron beam based spectroscopies. The measurements were performed using the Hitachi S-3000N Variable Pressure Scanning Electron Microscope (SEM) integrated with a NORAN 7 EDS/EBSD system, the Hitachi S-4800 II Field Emission Scanning Electron Microscope (FESEM), and the Hitachi H-9500 High-Resolution Transmission Electron Microscope (HRTEM) all located in the Characterization Center for Materials and Biology (CCMB) laboratory at the University of Texas at Arlington (UTA). The data assisted in the characterization of the crystal structure and chemical composition of the zeolite samples. The properties determined were used in calculations to estimate the fraction of positrons that will diffuse to the internal surfaces of the zeolite and to provide insight into the possible outcomes of the positron experiments.

TABLE OF CONTENTS

LIST OF ILLUSTRATIONS

Figure Page

LIST OF TABLES

Table Page

LIST OF GRAPHS

Graphs Page

CHAPTER ONE

Introduction

1.1 Overview

This thesis will report on the characterization of a clinoptilolite zeolite ($Na_3[Al_3Si_{15}O_{36}]12H_2O$) using Energy-dispersive X-ray spectroscopy (EDX/EDS) for chemical analysis, low energy Secondary Electron (SE) analysis for three-dimensional imaging and topography, and Transmission Electron Microscopy (TEM) for two-dimensional imaging at the angstrom level. The goal of this work is to provide additional information to be used in conjunction with data obtained using Positron-annihilation-induced Auger Electron and gamma Spectroscopy. The data obtained will also assist in the characterization of the crystal structure and chemical composition of the internal surfaces of the porous material. The results will be used to estimate the fraction of positrons that will diffuse to the internal surfaces of the zeolite and to make predictions regarding the possible outcomes of positron experiments.

1.2 Motivation for the Study of Zeolites Using Positron Spectroscopy

Zeolites are porous minerals which have been studied for centuries because of their useful properties. Today, more zeolites are synthesized than occur naturally; with some 245 known frameworks known. As of 2018, 40 of these frameworks occurred naturally (IZA-SC, 2017). Zeolites make good catalysts, among many other things, and are also classified as an adsorbent and molecular filter. They are used in the medical field for detoxification and water purification. Others have household use such as in kitty litter. In this application, zeolites trap the ammonium in the cat urine and prevent it from become ammonia gas (IMPS, 2019). The mineral can also be used in the environment to remove pesticides, radioactive metals, and heavy metals, such as mercury, cadmium, lead, and arsenic (Touchstone, 2011).

Millions of zeolite structures are theoretically possible; making research in this field a monumental but fascinating task.

1.3 Zeolite Structure

A zeolite can be formed naturally or can be synthesized. One of the defining properties of a zeolite is that the pores and cavities within the material are of consistent size; although there are some minor variations in the structure. There are elements within a zeolite lattice structure that are interchangeable while maintaining its name and classification. For instance, the clinoptilolite zeolite that is the focus of this study has a chemical formula of $\boldsymbol{Na_3[Al_3Si_{15}O_{36}]12H_2O}$. The chemical formula can be expressed more generally as:

$$\boldsymbol{(Na,K,Ca)_{2-3}\ Al_3\ (Al,Si)_2\ Si_{13}O_{36}\cdot 12H_2O};$$

where the elements in parenthesis are interchangeable. This means that the lattice structure of this zeolite may have some variations from another lattice structure while both lattices belonging to the same zeolite crystal. Zeolite frameworks exist in many different forms. Diagrams for representative Zeolite Frameworks of Type A, Y, L, and ZSM-5 D may be found in Zheng et al, 2012.

One of the methods used to remove unwanted material using zeolites is by means of **adsorption**. Zeolites can act as a molecular sieve which can adsorb certain molecules, compounds, or cations.

A second method by which zeolites can be used to remove unwanted material is by means of **filtration** (Advameg, 2019). An example would be water purification for fish farms, where the water can become polluted very quickly (Lenntech, 1998). Since the size of pores and cavities are more or less consistent, the zeolite can remove unwanted molecules and atomic clusters, as long as the size of the atomic clusters is larger than the pore size. The material that is not meant to be filtrated, in this case water, is smaller than the pore size. Thus, zeolites can be used for selective targeting of the impurities based on their sizes.

1.4 Zeolite Sample Specifications from Vendor

KMI Zeolite initially provided a sample information sheet included here in Table 1.4.1 and Table 1.4.2.

Table 1.4.1 Sample Data Sheet Information From KMI Zeolite (KMI, 2018)			
Chemical Formula:	Na6[Al6Si30O72]24H2O	Bulk Density:	45 – 54 lbs./ft3
Clinoptilolite Content:	97%+	pH stability:	3.0 – 10.00
Form:	Granules and Powders	Hardness:	4.0 – 5.0 Mohs
Pore Diameter:	4.0 – 7.0 angstroms	Swelling Index:	Nil
Specific Gravity:	1.89	Cation Exchange Capacity (CEC):	1.6 – 2.0 meg/g ($1\ Eg = 10^{18}\ g$)
Specific Surface Area:	40m2/g		

There are a few things to note from the data on Table 1.4.1 above:

- The "Pore Diameter" is in between 4 and 7 angstroms and will preferentially trap positrons. This means that there is some variation in the zeolite structure.

- The "Clinoptilolite Content" is a reference to its purity and that is greater than 97%. This indicates that there are some impurities already within the clinoptilolite sample. This impurities were either mined right along with the sample or could have been accidentally introduced into the sample during the refining process.

Table 1.4.2 Chemical Analysis from KMI Zeolite (KMI, 2018)								
SiO2	Al2O3	Fe2O3	CaO	MgO	Na2O	K2O	MnO	TiO2
66.7%	11.48%	0.9%	1.33%	0.27%	3.96%	3.42%	0.025%	0.13%

The "Chemical Analysis" on Table 1.4.2, above, shows elements that are not part of the chemical formula, such as iron (Fe), magnesium (Mg), and manganese (Mn).

1.5 Clinoptilolite Zeolites

The manufacturer provided chemical formula of the clinoptilolite zeolite material is $\boldsymbol{Na_3[Al_3Si_{15}O_{36}]12H_2O}$. The basic elements in the clinoptilolite structure are silicon (Si), aluminum (Al), and oxygen (O). When oxygen is combined with silicon or oxygen with aluminum, there are three types of structures that are likely to form. These structures are a silica tetrahedral (SiO_4), an alumina tetrahedral (AlO_4), or an alumina octahedral (AlO_6). In a clinoptilolite zeolite, these tetrahedrons will align themselves to form a caged structure. In this framework, each silicon, or aluminum, atom is surrounded by four oxygen atoms. The resulting tetrahedral can arrange themselves into many patterns, usually leaving a cavity where adsorption may takes place. The pore size can range from four to seven angstroms, according to KMI Zeolite (2018). This type of framework is referred to as a heulandite (IZA-SC, 2017). A diagram of the tetrahedral framework of a clinoptilolite zeolite may be found at the website: https://www.rotamining.com/clinoptilolite/ .

The Lewis dot diagram of the silica tetrahedral (SiO_4) and an alumina tetrahedral (AlO_4) (Hsieh, 1996) suggest that a clinoptilolite zeolite will have a negative surface potential. These un-bonded electrons are not shared among multiple atoms. Therefore, the clinoptilolite zeolite is an insulator and will not conduct electricity under normal circumstances; a fact that becomes important when running the sample through the electron microscope.

Structural diagrams and data may be found in The Database of Zeolite Structures published by the Structure Commission of the International Zeolite Association: http://www.iza-structure.org/databases/

Table 1.5.1 Crystal Data for Clinoptilolite Database of Zeolite Structures (IZA-SC, 2017)			
Space Group:	C 1 2/m 1	(#12)	
Cell parameters:	a = 17.662 Å	b = 17.911 Å	c = 7.407 Å
	α = 90°	β = 116.4°	γ = 90°

Table 1.5.2 Coordinate Crystal Data for Clinoptilolite Database of Zeolite Structures (IZA-SC, 2017)						
Atom	**Form Factor**	**x**	**y**	**z**	**PP**	**B(iso)**
NA1	Na	0.1428	0	0.667	0.36	5.49
NA2	Na	0.0393	0.5	0.21	0.1	3.13
K3	K	0.2413	0.5	0.049	0.44	5.1
MG4	Mg	0	0	0.5	0.1	1.1
CA1	Ca	0.1428	0	0.667	0.06	5.49
CA2	Ca	0.0393	0.5	0.21	0.25	3.13
SI1	Si	0.17906	0.16943	0.0963	0.83	1.07
SI2	Si	0.21334	0.41099	0.504	0.69	1.1
SI3	Si	0.20846	0.19034	0.7153	0.87	1.01
SI4	Si	0.06623	0.29837	0.4148	0.89	1.09
SI5	Si	0	0.21651	0	0.9	1.11
AL1	Al	0.17906	0.16943	0.0963	0.17	1.07
AL2	Al	0.21334	0.41099	0.504	0.31	1.1
AL3	Al	0.20846	0.19034	0.7153	0.13	1.01
AL4	Al	0.06623	0.29837	0.4148	0.11	1.09
AL5	Al	0	0.21651	0	0.1	1.11
O1	O	0.1959	0.5	0.4574	1	2.39
O2	O	0.2336	0.1204	0.6144	1	2.47
O3	O	0.185	0.1551	0.8559	1	2.64
O4	O	0.2333	0.1041	0.2509	1	2.37
O5	O	0	0.3232	0.5	1	2.64
O6	O	0.0808	0.1627	0.0555	1	1.96
O7	O	0.1268	0.2317	0.5492	1	3.05
O8	O	0.0122	0.2702	0.1856	1	2.48
O9	O	0.2123	0.252	0.186	1	2.31
O10	O	0.1188	0.3718	0.4148	1	2.42
H2O1	O2-(H2O)	0.211	0.5	-0.033	0.38	6.2
H2O2	O2-(H2O)	0.084	0	0.888	0.44	14.6
H2O3	O2-(H2O)	0.0777	0.4206	0.964	1	9.5
H2O4	O2-(H2O)	0	0.5	0.5	1	7.4
H2O5	O2-(H2O)	0	0.095	0.5	0.76	22.1
H2O6	O2-(H2O)	0.073	0	0.249	0.84	19.1
H2O7	O2-(H2O)	0.096	0	0.756	0.42	10.2

1.6 Outline of the Thesis Work

The remainder of this thesis describes the methods used to further characterize the as received zeolite materials and the results obtained using these methods. The thesis includes calculations aimed at helping to provide an estimate of the efficacy of a novel spectroscopic technique. These techniques employed a low energy beam of positrons in the characterization of the internal surfaces of porous zeolite materials.

The primary methods of characterization used in this thesis employed electron microscopes. An electron microscope equipped with an Energy Dispersive X-ray (EDX) instrument was used in obtaining the chemical composition of the clinoptilolite. The chemical composition obtained using EDX is compared with the chemical composition provided by KMI Zeolite. A similar comparison was carried out between the vendor specified atomic structure of the sample with a determination of the crystal structure obtained using the electron microscopy. An inverse Fourier transform was used in order to determine the individual frequencies of the diffracted X-ray waves. This technique is also a way to determine bond lengths and orientation, which can be used to fully characterize the sample.

A number of types of instruments were used in the characterization of the clinoptilolite zeolite; among these are two Scanning Electron Microscopes (SEM) and the High Resolution (HR) Transmission Electron Microscope (TEM). The instruments used in this thesis were housed in the Characterization Center for Materials and Biology (CCMB) at the University of Texas at Arlington (UTA).

The organization of the rest of the thesis is as follows: Chapter Two describes the characterization of the candidate Zeolite sample material using scanning electron microscopy. Chapter Three describes the characterization of the candidate zeolite sample material using Transmission Electron Microscopy. Chapter Four gives the Makhovian profile for the clinoptilolite in detail and, also, background information on positrons and the anti-matter instruments at UTA. In Chapter Five, the conclusions for all the chapters are laid out.

Figure 1.6.1

The clinoptilolite zeolite in granule form as provided by KMI Zeolite. Dimensions of the area shown: Approximately 7.5 cm. x 12.5 cm.

CHAPTER TWO

Characterization of the Zeolite Sample Candidate Material Using Scanning Electron Microscopy

2.1 Overview

This chapter contains the data collected by the scanning electron microscopes (SEMS). The SEM data was used to help verify the data provided by KMI Zeolite and to develop background knowledge regarding the samples useful in the interpretation of the results obtained in planned positron spectroscopic studies. A second reason for the study was to investigate the nature and degree of impurity content in the samples.

A Hitachi S-3000N Variable Pressure Scanning Electron Microscope (VPSEM) was employed to conduct chemical analysis on the sample. It uses a built-in Energy Dispersive X-ray (EDX) instrument that can be used in sequence with the imaging system; without a need to reload the sample. The penetration depth of the EDX system is dependent on the energy of the incident beam. In the measurements reported here, the beam energy used was no more than 30 kilovolts. Several images were also attained using the Hitachi S-4800 II Field Emission Scanning Electron Microscope (FESEM) which uses low energy Secondary Electron analysis for three-dimensional imaging and topography (ThermoFisher, 2019). These two instruments sit at the Characterization Center for Materials and Biology (CCMB) at the University of Texas at Arlington (UTA) and are available for use by most students provided they have the proper training (CCMB, 2019).

The following are the procedures used to characterize the clinoptilolite when using these SEM's and the results from those procedures.

2.2 Sample Preparation

Clinoptilolite preparation steps for use in a scanning electron microscope:

1) Basic laboratory safety precautions were employed including protective clothing, eye protection, and maintaining a clean area to work in order to reduce contamination. Likewise, all other equipment was either brand new or had been cleaned and sterilized. Latex gloves were used when possible to reduce the risk of contaminating the sample with impurities.
2) The sample was crushed with a mortar and pestle into powder form. Enough of the material was crushed to produce multiple samples.
3) Once crushed, the clinoptilolite powder was mixed in a test tube with ethanol to produce a mixture. Proper dispersion was not achieved at this point.
4) The test tube and its contents were sonicated for several minutes. Sonication was done at 5 to 10 minute intervals to prevent the plastic test tube from melting.
5) The test tube was allowed to sit for a couple of hours and then checked to confirm that the clinoptilolite had properly dispersed.
6) On the first attempt, the clinoptilolite powder did not appear to have dispersed properly. The clinoptilolite was then dried in the oven, re-crushed, and re-sonicated until proper dispersion was achieved.

Figure 2.2.1

Plastic Test Tube with Dispersed Sample

7) A pipet was used to extract the mixture from the top of test tube and transport it onto the platinum substrate.
8) The sample was left to bake under moderate heat for a couple of days to attempt to remove impurities that had been adsorbed inside the material.

9) The unused crushed material was stored in a vacuum chamber to prevent further contamination over time.

The sample was kept under heat until it was time for the appointment to use the SEM's at the CCMB at UTA. A small vacuum desiccator was used to transport the clinoptilolite to the lab; although it is important to remember that due to the adsorbing nature of the clinoptilolite, it may not have been possible to completely avoid the adsorption of some impurities from the environment.

This sample preparation process described above has another beneficial effect. Any clinoptilolite that has adsorbed impurities, such as heavy metals, will have a greater density and will have also have a greater chance to collect at the bottom of the test tube. Therefore, if extracting the sample from the dispersed material towards the top of the test tube, may have resulted in a purer sample than what was originally delivered.

2.3 Issues Related to Sample Preparation and Sample Charging

The SEM's used in this characterization are able to accept a fairly large sample sizes; approximately 150 millimeters in diameter. There are other things to consider such as the sample charging. The sample is exposed to a beam of electrons from the SEM's electron gun; usually in the energy range of no more than 30 kilovolts. If the sample is a conductor, then any electrons, that are not part of backscattered electrons (BSE) or the SE process, will conduct around the sample and eventually make their way to a ground. If the sample is an insulator, however, then the sample will collect a charge. The charge on the sample can create inhomogeneous electric fields which can cause distortions in the image. Examples of images with distortion are shown in Figures 2.5.7, 2.5.8, and 2.5.9.

The following two images show the substrate at different stages of this process. Figure 2.3.1 shows a prepared substrate baking in an oven while Figure 2.3.2 shows a different prepared substrate that has been attached to the SEM's sample holder. The sample on the substrate in Figure 2.3.1 proved to be too thick to prevent the charging effect. The sample in the mixture had to be dried, further crushed, and re-sonicated in order to get the clinoptilolite to disperse correctly. Once the sample disperses correctly,

the mixture should appear murky, but towards the clear side as shown in Figure 2.2.1, and will produce a substrate that looks like the one shown in Figure 2.3.2.

Figure 2.3.1 (left)

Crushed and Sonicated Clinoptilolite over a Platinum Substrate.

The substrate is sitting over aluminum foil and baking overnight.

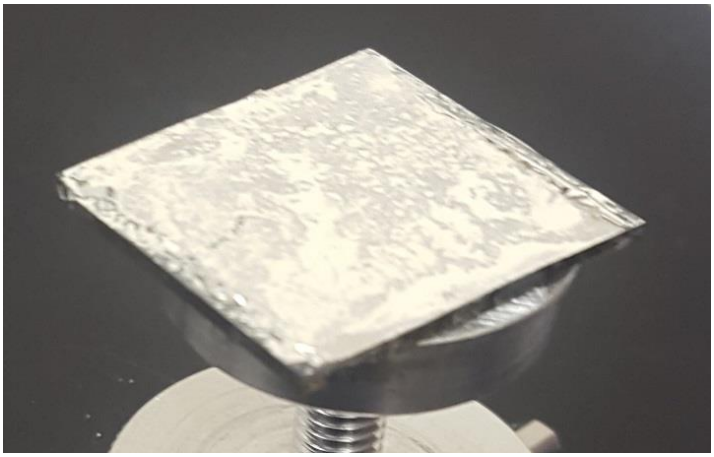

Figure 2.3.2 (right)

Crushed and Sonicated Clinoptilolite over a Platinum Substrate.

Substrate is attached to the scanning electron microscope's sample holder.

2.4 Issues Related to Sample Preparation and Sample Structure

In order to reduce thickness and prevent sample charging in the SEM, the sample was crushed and sonicated. There are some articles that warn against doing either of these things to clinoptilolite (Solyman, 2013), as it might break apart the crystal structure. Unfortunately, there is no other method that can used to prepare this particular sample for use in an SEM. Ergo, the conundrum becomes that crushing and sonicating the sample is necessary to prevent charging but it may also destroy the crystal structure.

2.5 Hitachi S-4800 FESEM Images

This section contains the images taken with the Hitachi S-4800 Field Emission Scanning Electron Microscope. The Hitachi S-4800 FESEM is likely to give the better image quality out of the two SEM's and therefore it was chosen for the imaging process in this characterization. To be thorough and for better reference, the images were taken at increasing magnifications; encompassing the full range of the FESEM's imaging capabilities. The last set of images, Figures 2.5.7, 2.5.8, and 2.5.9, are examples of distortion that was likely caused as a result of the sample charging. It is important to note that these images, although 2D images themselves, are an attempt to show the topography in 3D. The objects in the images show depth illustrated by black and white shading; the objects are illuminated much in the same way as if a light beam was aimed at these features.

Figures 2.5.1, 2.5.2, 2.5.3, and 2.5.4 were taken at x2.22k, x5.00k, x11.0k, and x20.0k magnifications respectively. At these magnifications, the FE SEM performed well and produced clear and sharp images of the clinoptilolite. Please note the scales on the lower right hand corner for each image, 20 μm, 10 μm, 5 μm, and 2 μm, also listed respectively. This indicates that the detail and features in the images are in the micron to tens of microns range. The datasheet KMI zeolite provided indicate that the pore size of the sample is approximately from 4.0 to 7.0 angstroms. Therefore, Figures 2.5.1, 2.5.2, 2.5.3, and 2.5.4, do not show any discernible evidence that confirm that this is clinoptilolite and greater magnification are needed.

The two images, Figures 2.5.5 and 2.5.6, were taken at x60.0k and x110k magnification respectively. As one can see by the scales on the lower right hand corner, magnification at this level will produce details and features that are in the scale of hundreds of nanometers. It is worth noting that zooming in at the scale opens up a whole new topography. Unfortunately, this is not enough detail to view features at the 4.0 to 7.0 angstroms range, such as the clinoptilolite pores. Also, at this magnification, blurriness and image distortion begin to materialize in the images.

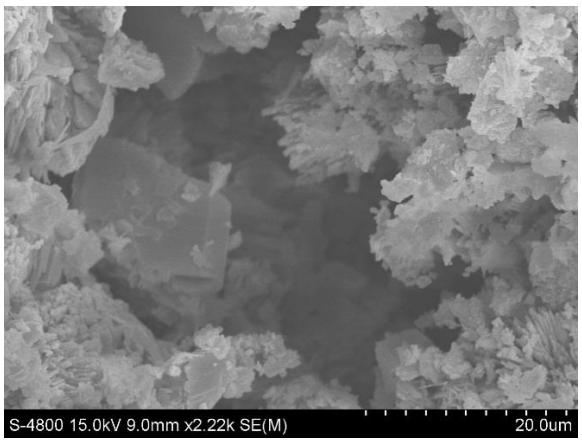

Figure 2.5.1 (left)

Hitachi S-4800 FESEM Image of Clinoptilolite at x2.22k magnification.

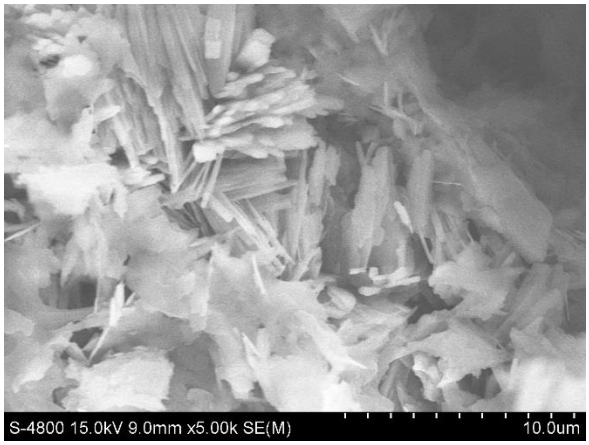

Figure 2.5.2 (right)

Hitachi S-4800 FESEM Image of Clinoptilolite at x5.00k magnification.

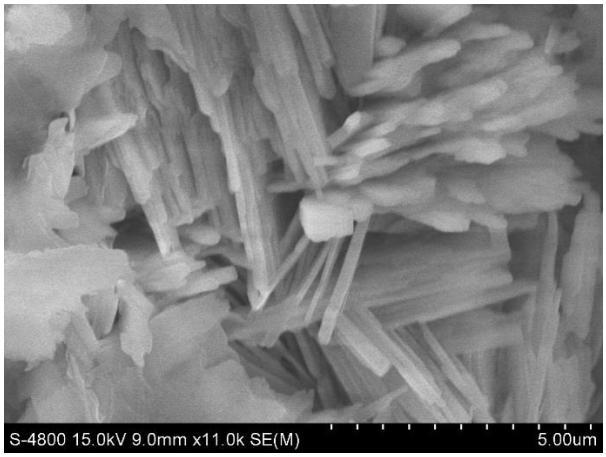

Figure 2.5.3 (left)

Hitachi S-4800 FESEM Image of Clinoptilolite at x11.0k magnification.

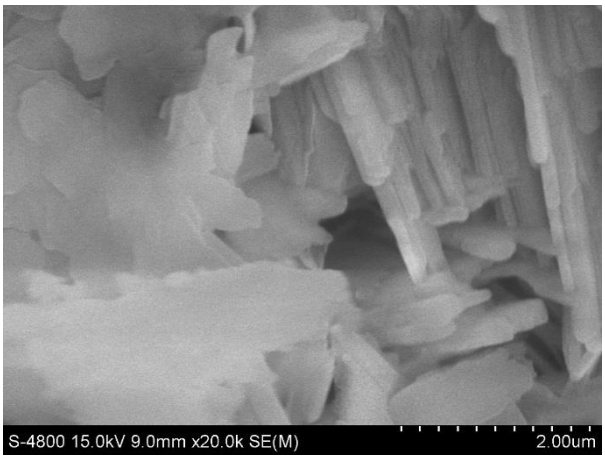

Figure 2.5.4 (right)

Hitachi S-4800 FESEM Image of Clinoptilolite at x20.0k magnification.

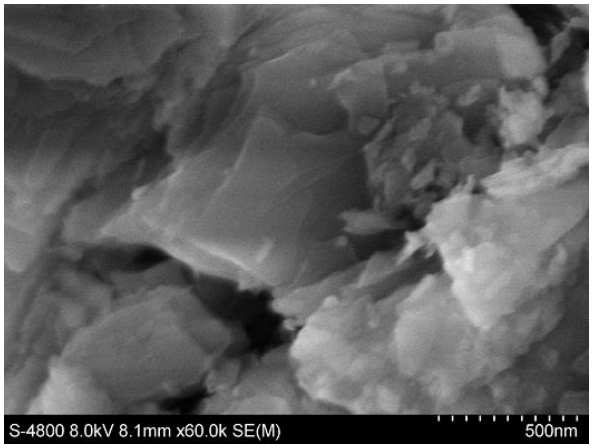

Figure 2.5.5 (left)

Hitachi S-4800 FESEM Image of Clinoptilolite at x60.0k magnification.

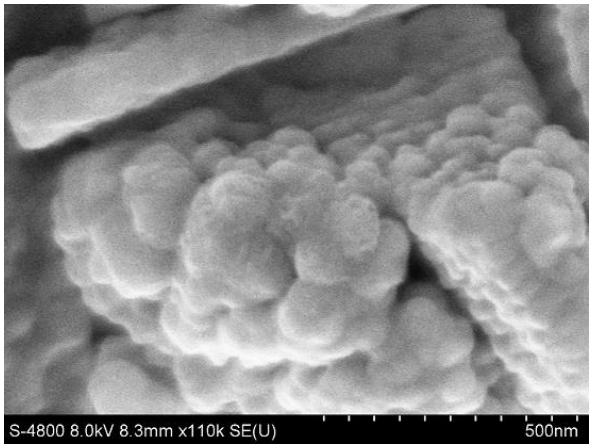

Figure 2.5.6 (right)

Hitachi S-4800 FESEM Image of Clinoptilolite at x110k magnification.

Finally, Figures 2.5.7, 2.5.8, and Figure 2.5.9 were taken at magnifications x250k, x300k, and x301k respectively. One can see by the scales on the lower right hand side of the images that the size of details and features of the clinoptilolite are on the order of tens of nanometers. This is still not enough magnification in order to discern any part of the atomic structure.

As one can see, these set of images are completely distorted. Figures 2.5.7 and 2.5.8 have horizontal lines across the entire image while Figure 2.5.9 is blurry to the point no features are discernable. The clinoptilolite is an insulator and it is likely that it became charged, resulting in interference with the SEM's imaging instrumentation while also causing the distortions in the images. This type of interference ultimately reduces the maximum resolution able to be attained.

There was an attempt to correct the issue by using a method in which the sample is coated with a layer of conducting metal. A CrC-100 Sputtering System, housed in the CCMB at UTA was used to apply a coating of silver (Ag) to the sample. Although the silver coating did help produce sharper images, the Hitachi S-4800 FESEM was not able to magnify much further without running into the same charging problems.

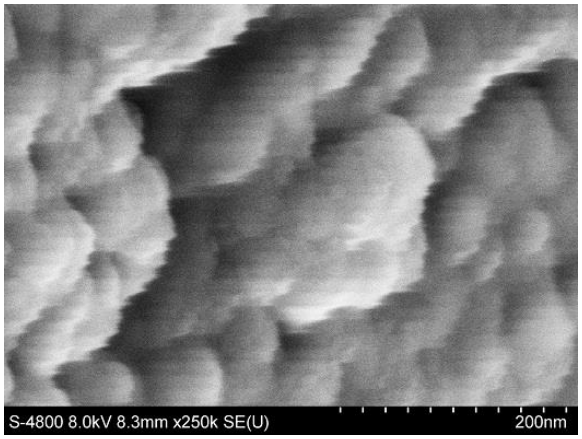

Figure 2.5.7 (left)

Hitachi S-4800 FESEM Image of Clinoptilolite at x250k magnification.

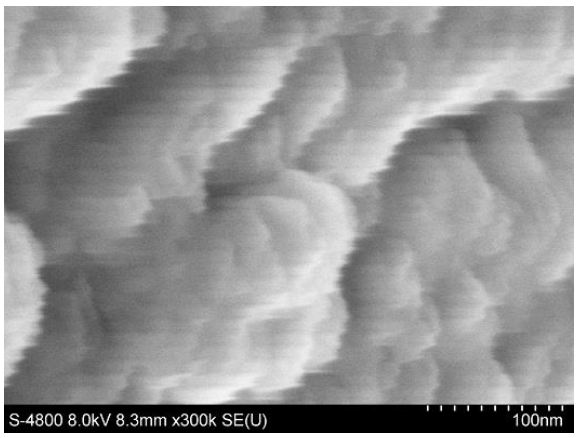

Figure 2.5.8 (right)

Hitachi S-4800 FESEM Image of Clinoptilolite at x300k magnification.

The Hitachi S-4800 FESEM is capable of greater magnifications provided the sample is a conductor. While imaging the clinoptilolite, the SEM was used at a range of 8 to 15 kilovolts; but it is capable of accelerating electrons to 30 kilovolts. However, the images shown in this section show the maximum magnification that can be achieved with this instrument because the sample is an insulator and it is building up charge while inside the SEM's vacuum chamber.

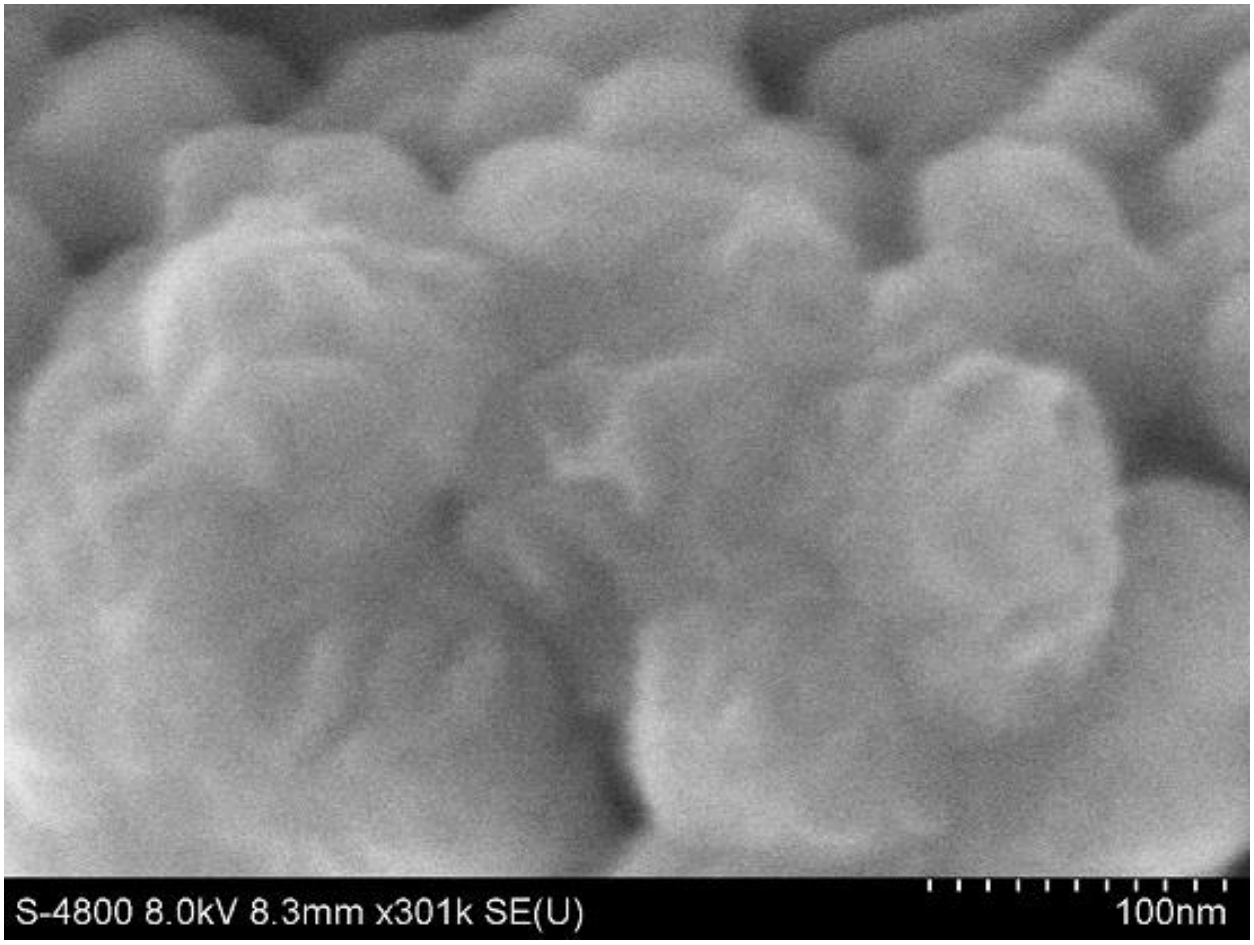

Figure 2.5.9

Hitachi S-4800 FESEM Image of Clinoptilolite at x301k magnification.
Sample charging is noticeable here as it has caused blurriness and distortion in the image.

2.6 Hitachi S-3000N VPSEM Chemical Analysis

The results of the chemical analysis were in good agreement with the data that KMI Zeolite provided. **The atoms that make up the main components of the clinoptilolite, oxygen (O), aluminum (Al), and silicon (Si), do appear in the appropriate percentages in the Hitachi S-3000N VPSEM chemical analysis.** Table 2.6.1 shows the chemical analysis provided by KMI Zeolite. Notice that it is given in terms of molecules, such as aluminum oxide (Al_2O_3) and iron (III) oxide (Fe_2O_3) for example, not individual atoms. Below that, Tables 2.6.2 and

2.6.3, were created from the EDX data collected from the Hitachi S-3000N VPSEM; the EDX data was also converted into Graphs 2.7.1 and 2.7.2.

Table 2.6.1 Chemical Analysis Provided by KMI Zeolite								
SiO2	Al2O3	Fe2O3	CaO	MgO	Na2O	K2O	MnO	TiO2
66.7%	11.48%	0.9%	1.33%	0.27%	3.96%	3.42%	0.025%	0.13%

Table 2.6.2 EDX Chemical Analysis Using Hitachi S-3000N VPSEM (before coating)							
Element	N	O	Na	Mg	Al	Si	Ca
Wt %	00.00	65.57	05.00	00.62	05.50	22.94	00.37
At %	00.00	76.30	04.05	00.48	03.80	15.20	00.17

Table 2.6.3 EDX Chemical Analysis Using Hitachi S-3000N VPSEM (after coating)									
Element	C	O	Al	Si	Ag	Ca	Fe	Co	U
Wt %	04.55	08.41	01.04	06.70	67.68	06.57	00.90	00.00	04.15
At %	18.88	26.19	01.93	11.89	31.27	08.17	00.80	00.00	00.87

Something important to note is that elements with an atomic number equal to or less than five (boron) cannot be detected with EDX chemical analysis, such as the hydrogen in water (ResearchGate, 2015). Ergo, when looking at Graph 2.7.1, some of the oxygen listed may be part of water molecules still adsorbed within the material. Another possible source of uncertainty is the degree to which the sample adsorbs oxygen from the air, as the sample was exposed to the atmosphere while it is removed from the oven and placed in the vacuum desiccator and when it is removed from the vacuum desiccator and loaded into the electron microscope. While some adsorbed oxygen may be removed through desorption resulting from the vacuum environment of the electron microscope it is possible that some of the oxygen adsorbed during the sample transfer process remains.

Nitrogen does show up on the Hitachi S-3000N VPSEM chemical analysis as 0.00% which indicates traces for the gas in the thousandths of a percent. Nitrogen does not show in the KMI Zeolite chemical analysis so this is possibly indicative of the amount of gas adsorbed by the sample in its brief contact with the atmosphere.

There are elements (manganese (Mn), iron (Fe), potassium (K), and titanium (Ti)) that appear in the chemical analysis provided by KMI Zeolite at the level of less than 1%. These are missing from the chemical analysis taken by the Hitachi S-3000N VPSEM EDX system possibly due to the sensitivity limits of the measurements.

Graph 2.7.2 shows the EDX taken after coating the sample with silver. This was done as a test, although the graph clearly shows that any useful information will be skewed after coating. Carbon (C), cobalt (Co), and uranium (U) were also detected but were not listed in any of the previous chemical analysis. One theory is that the coating process somehow contaminated the sample with these elements; although further testing is needed to say with certainty.

This also indicates that two substrates with the sample are needed in order to obtain data from the clinoptilolite using the SEM's, one for EDX analysis and the other for imaging purposes only.

2.7 Conclusions Pertaining to the SEM Results

The Hitachi S-3000N VPSEM and the Hitachi S-4800 II FESEM proved to be useful in the characterization process. The chemical analysis done by the Hitachi S-3000N VPSEM's EDX system were largely in agreement with chemical analysis provided by KMI Zeolite. However, there were limitations to the Hitachi S-4800 II FESEM's imaging quality due to charging.

EDX GRAPHED DATA

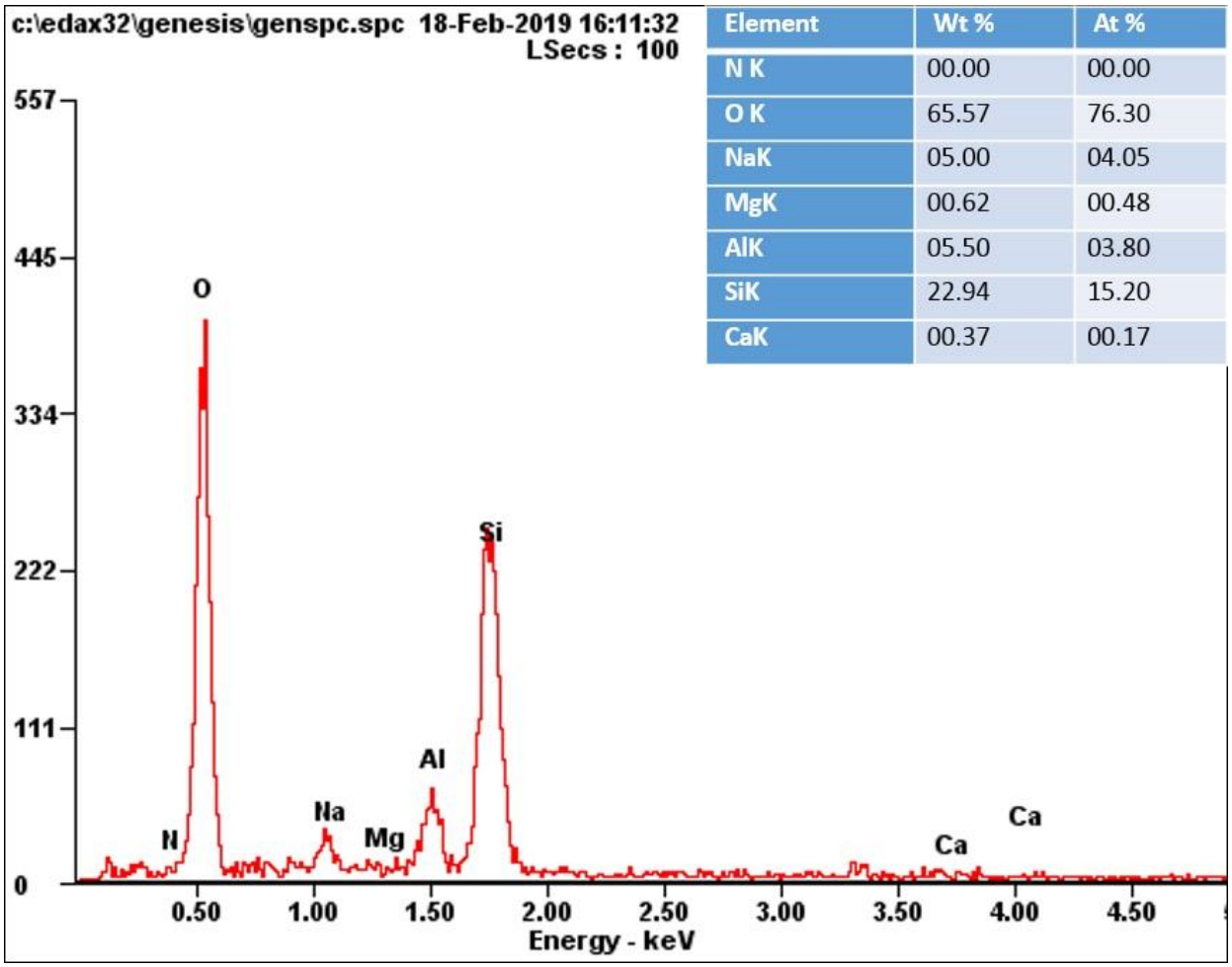

Element	Wt %	At %
N K	00.00	00.00
O K	65.57	76.30
NaK	05.00	04.05
MgK	00.62	00.48
AlK	05.50	03.80
SiK	22.94	15.20
CaK	00.37	00.17

Graph 2.7.1

Hitachi S-3000N VPSEM EDX Microanalysis Report
of Clinoptilolite over a Platinum Substrate.

The chemical composition is given in both weight percent and atom count percent.

(data collected before silver coating)

EDX GRAPHED DATA

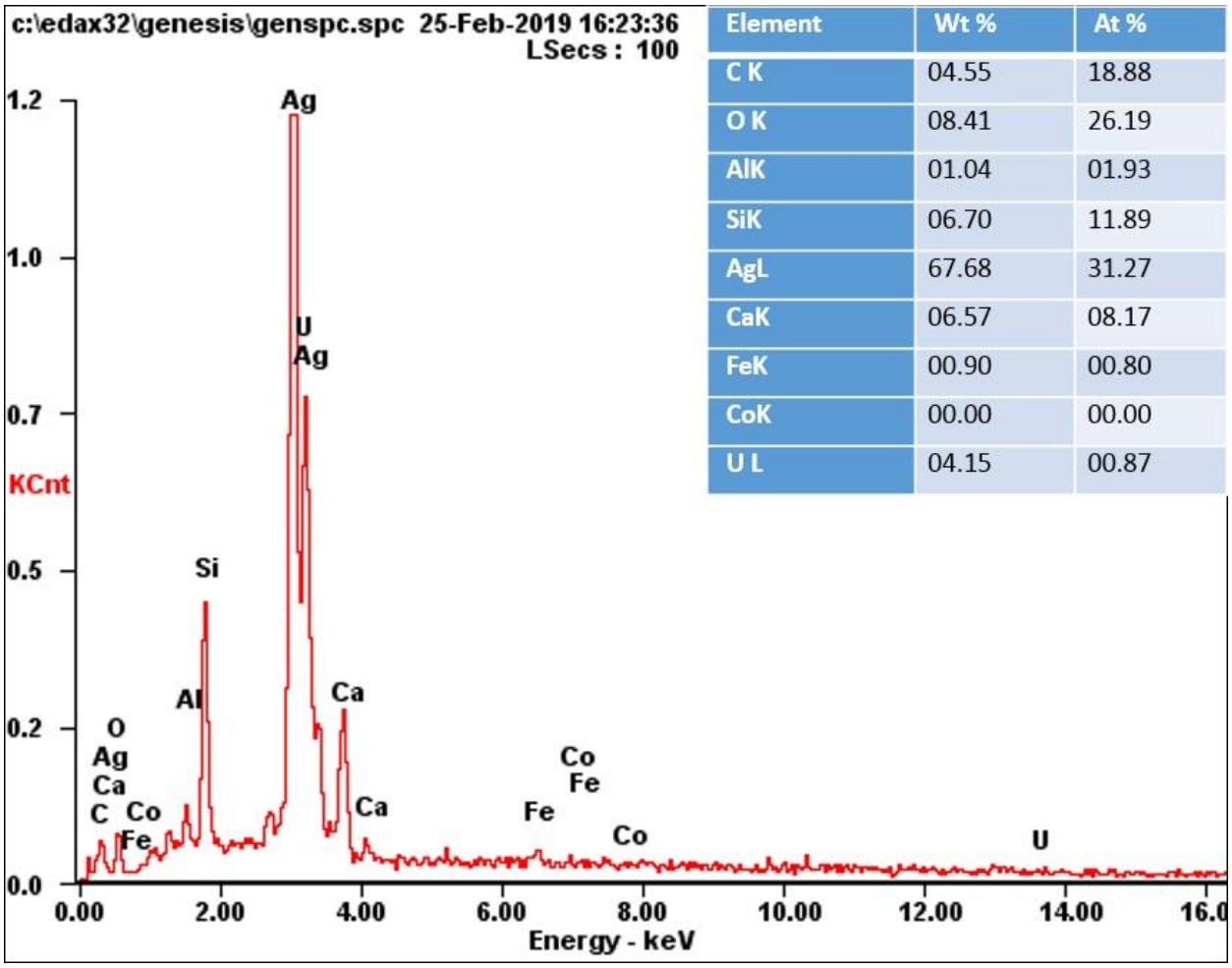

Element	Wt %	At %
C K	04.55	18.88
O K	08.41	26.19
AlK	01.04	01.93
SiK	06.70	11.89
AgL	67.68	31.27
CaK	06.57	08.17
FeK	00.90	00.80
CoK	00.00	00.00
U L	04.15	00.87

Graph 2.7.2

Hitachi S-3000N VPSEM EDX Microanalysis Report
of Clinoptilolite over a Platinum Substrate.

The chemical composition is given in both weight percent and atom count percent.

(data collected <u>after</u> silver coating)

CHAPTER THREE

Characterization of the Candidate Zeolite Sample Material Using Transmission Electron Microscopy

3.1 Overview

The chemical composition of the clinoptilolite was verified using Energy Dispersive X-ray (EDX) analysis, which was an instrument of the Hitachi S-3000N Variable Pressure Scanning Electron Microscope (VPSEM). The Hitachi S-4800 II Field Emission Scanning Electron Microscope (FESEM) imaging system was limited in the magnification that it could produce because of sample charging. Sample charging is described in chapter two of this thesis. The images, taken with the Hitachi S-4800 II FESEM, were not adequate for the identification of the crystal/lattice structure of the samples.

In order to obtain the higher resolution necessary for structural determination, the Hitachi H-9500 High-Resolution Transmission Electron Microscope (HRTEM), also located at the Characterization Center for Materials and Biology (CCMB) at the University of Texas at Arlington (UTA), was used as the third step in the characterization process. TEM's work by transmitting electrons through the sample therefore the problem of sample charging is completely eliminated. The Hitachi H-9500 HRTEM can zoom into an object up to 1.5 (10^6) times magnification; which is five times what the SEM's could do. At these magnifications, one is hopeful to be able to see detail in the angstrom range. It can also equipped with instrumentation which can perform Fast Fourier Transform (FFT) analysis; which can be used to further verify the characterization of the sample. This capability was not available with either of the SEM's.

Also, the Hitachi H-9500 HRTEM comes equipped with an EDX instrument which can be used to verify the Hitachi S-3000N VPSEM's chemical analysis. This particular HRTEM can accelerate electrons to a maximum of 300 kilovolts; so the HRTEM's EDX system can prove deeper into the sample. For comparison, the SEM's at the CCMB could be operated at a maximum of 30 kilovolts by design.

The following sections are the procedures used to characterize the clinoptilolite when using the Hitachi H-9500 HRTEM and the results from those procedures.

3.2 Sample Preparation

As far as clinoptilolite is concerned, the steps used in the TEM sample preparation were almost identical to those used to prepare the samples for use in the SEM's. These instructions were given in detail in Section 2.2, of this thesis. The main difference in preparation was that when extracting the dispersed mixture with the pipet, from the top of the test tube, one would transport the sample to a TEM grid instead platinum substrate. Afterwards, one would bake the TEM grid in the oven just the same as the instructions indicate for the platinum substrate.

The TEM grids are predominantly copper and they are very similar to the one shown below in Figure 3.2.1. They are 3 millimeters in diameter and are very difficult to handle. Fine point tweezers have proven to be the best tool for handling these grids without causing damage to them (Jiang, 2009).

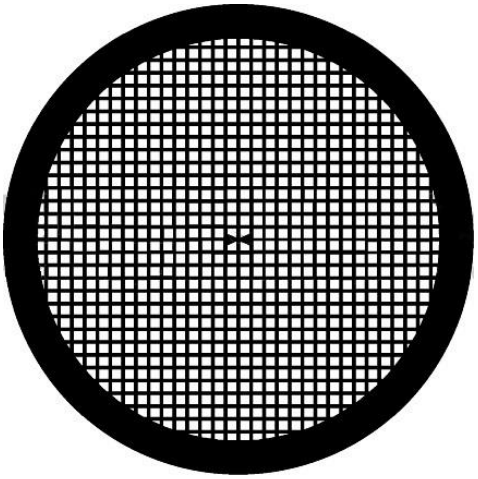

Figure 3.2.1 (left)

TEM Grid
(diameter: 3 millimeters)

(SPI, 2019)

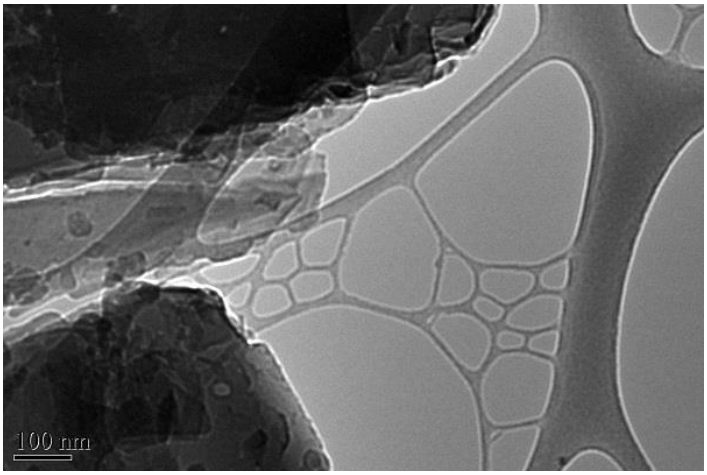

Figure 3.2.2 (right)

Clinoptilolite (the darker areas on the left)
Over Lacey Formvar Carbon Film

(Supported on the web-like structure on the right).

TEM's cannot transmit electrons through the thicker copper grid material. Consequently, the grid material shows as solid black in the images. Any sample material directly above the copper will also show as solid black and will not be viewable; so another method to hold up the sample is necessary.

The spaces between the Cu grid elements are spanned by a Lacey Formvar carbon film; which is pictured in Figure 3.2.2, on the right side of the image. The carbon film is the web-like structure and it is what actually holds up the sample; in this case clinoptilolite. The clinoptilolite is shown on the left side of the image, of Figure 3.2.2, and it is represented by the darker areas. A 100 nanometers bar in the lower left corner of the image indicates the scale. The following table contains the TEM grid specifications:

Table 3.2.1 Transmission Electron Microscope Grid Specifications (Tedpella, 2019)	
PELCO NetMesh Grids	Lacey Support Films: 01883-F
300 mesh	Lacey Formvar/Carbon
Copper approximate grid hole size: 63μm	

It is possible that the EDX system will pick up carbon and copper, the TEM grid's only components, in addition to the elements that have already been identified. Both of these elements have an atomic number greater than boron, therefore they are detectable by EDX analysis (ResearchGate, 2015). Also, copper and carbon are both missing from the KMI zeolite chemical analysis and the EDX analysis performed by the Hitachi S-3000N VPSEM; ergo, if these elements are detected by the Hitachi H-9500 HRTEM's EDX, then the source of these detections could only be the TEM grid.

3.3 Sample Charging and the Preparation Conundrum

Sample charging, as it relates to the SEM's and this sample, is covered in detail in Sections 2.2.1 and 2.2.2 and Section 2.3. In the Hitachi H-9500 HRTEM, however, electrons are transmitted right through the sample at high energy. Consequently, sample charging

does not become an issue. The thickness of the sample has to be reduced enough, though, so that the electrons are able to be transmitted. This HRTEM will accelerate electrons to a maximum of 300 kilovolts. If the electrons cannot be transmitted through the sample using the maximum energy, then the sample thickness must be reduced. The preparation conundrum resurfaces again but for a different reason. Reducing the thickness of the clinoptilolite requires the use of sample preparation methods such as crushing and sonicating. However, as stated in chapter 3 on this thesis, there are some articles that warn against doing either of these things to clinoptilolite (Solyman, 2013), as it might break apart the lattice structure. Thus, the preparation conundrum is slightly different when using clinoptilolite in a HRTEM: crushing and sonicating the sample is necessary to reduce the sample's thickness but it may also destroy the lattice structure.

3.4 Hitachi H-9500 HRTEM Chemical Analysis

The results of the Hitachi H-9500 HRTEM EDX chemical analysis did concur with the data that KMI Zeolite provided and with the chemical analysis performed by the Hitachi S-3000 VPSEM. **The Clinoptilolite's main elemental components, oxygen (O), aluminum (Al), and silicon (Si), appear in the appropriate percentages for all three of these chemical analyses.** For easier comparison of the data, all EDX data that has was shown in Section 2.6 has been reprinted alongside the HRTEM EDX data in this section. Table 3.4.1 shows the chemical analysis provided by KMI Zeolite given in terms of molecules; such as aluminum oxide (Al_2O_3) and iron (III) oxide (Fe_2O_3). Below that, Tables 3.4.2 and 3.4.3, were created from the EDX data collected from the Hitachi S-3000N VPSEM; before and after coating respectively. Lastly, Table 3.4.4 shows the EDX data taken with the Hitachi H-9500 HRTEM. The EDX data for Table 3.4.4 was converted into graph format and is shown on Graph 3.4.1.

The EDX systems, on both the Hitachi S-3000N VPSEM and the Hitachi H-9500 HRTEM, are different from each other as they were built for different instruments. Fundamentally, though, they are identical and work on the same principles. Hence, the EDX chemical analysis systems on both of these instruments cannot detect elements with an atomic number equal to or less than five; which is boron (B) (ResearchGate, 2015). The reason is because there are not enough electrons in this elements to fill the outer shells.

Only the K-shell gets completely filled and the L-shell only gets partially filled. Ergo, these first five elements lack the outer shells that an electron can drop down from and therefore the electron cannot release a high energy photon. It is the energy of the X-ray that is measured to determine which element it came from. Therefore, when looking at the data on Table 2.3.4, it is important to note is that the hydrogen in water cannot be detected with the EDX chemical analysis. Any oxygen detected, may be from water molecules, oxygen gas that have been adsorbed into the sample, or oxygen atoms chemical bound in the lattice structure. As discussed in Section 2.6, the contribution of oxygen gas and water molecules to the total oxygen detected is most likely negligible.

Table 3.4.1
KMI Zeolite Chemical Analysis

SiO_2	Al_2O_3	Fe_2O_3	CaO	MgO	Na_2O	K_2O	MnO	TiO_2
66.7%	11.48%	0.9%	1.33%	0.27%	3.96%	3.42%	0.025%	0.13%

Table 3.4.2
EDX Chemical Analysis Using Hitachi S-3000N VPSEM (before coating)

Element	N	O	Na	Mg	Al	Si	Ca
Wt %	00.00	65.57	05.00	00.62	05.50	22.94	00.37
At %	00.00	76.30	04.05	00.48	03.80	15.20	00.17

Table 3.4.3
EDX Chemical Analysis Using Hitachi S-3000N VPSEM (after coating)

Element	C	O	Al	Si	Ag	Ca	Fe	Co	U
Wt %	04.55	08.41	01.04	06.70	67.68	06.57	00.90	00.00	04.15
At %	18.88	26.19	01.93	11.89	31.27	08.17	00.80	00.00	00.87

Table 3.4.4
EDX Chemical Analysis Using Hitachi H-9500 HRTEM

Element	O	Zn	Al	Si	Cu
Wt %	51.20	01.90	04.00	34.30	08.60
At %	67.60	00.60	03.20	25.80	02.80

In section 2.6, it was noted that the elements such as manganese (Mn), iron (Fe), potassium (K), and titanium (Ti) were detectable by EDX analysis (Research Gate, 2015). These elements were present in the KMI Zeolite chemical analysis, but not in the chemical analysis performed by the Hitachi S-3000N VPSEM possibly due to the fact these elements were present in the sample in quantities below the detection limits of our measurements.

Also in Section 2.6, the detection of the elements Carbon (C), cobalt (Co), and uranium (U) was discussed. Their presence is most likely due to contamination during the coating process performed before the sample was loaded in the SEM. The TEM grid was not subjected to any sort of coating because of the nature of how TEM's function and operate. The electrons are transmitted through the sample and therefore the sample will not collect charge, eliminating the need for any coating. The data on Table 3.4.4 supports the theory, introduced in Section 2.6, that the contamination was introduced during the coating process as these elements were not detected by the Hitachi H-9500 HRTEM's chemical analysis.

Interestingly, Table 3.4.4 also shows the presence of zinc in the HRTEM EDX analysis. Zinc is not used in the TEM grids so they are not thought to be the source of the zinc. It is possible that zinc was deposited or released during the sample preparation process. Additional data would be necessary to confirm this conclusion.

One can also see on Table 3.4.4 that copper was detected. The main and only components of TEM grids that were used in the Hitachi H-9500 HRTEM are copper and carbon; so the detection of copper is no surprise. What was surprising was the absence of detected carbon. Figure 3.2.1 shows the copper grid and Figure 3.2.2 shows the carbon mesh that the clinoptilolite sat on; ergo, the presence of these elements has been verified. It is hypothesized that the low density of the Lacy Carbon film resulted in a C signal below the detection limits of the measurement. The Hitachi H-9500 HRTEM has two separate electron guns and the imaging electron gun sits at the very top of the instrument. The secondary electron gun used for EDAX sits of the side of the instrument. In order for the EDX beam to reach the TEM grid, the TEM's specimen holder must be tilted 17 degrees while inside the vacuum chamber. The software then allows for an area of the grid to be analyzed. Consequently there is a realignment and refocusing process that must be performed between taking an image and performing an EDX analysis, or vice versa. This

means that the image and the EDX analysis come from the same TEM grid but may not come from the same spot. The location in the image at which the EDX analysis was performed can only be approximated with the software.

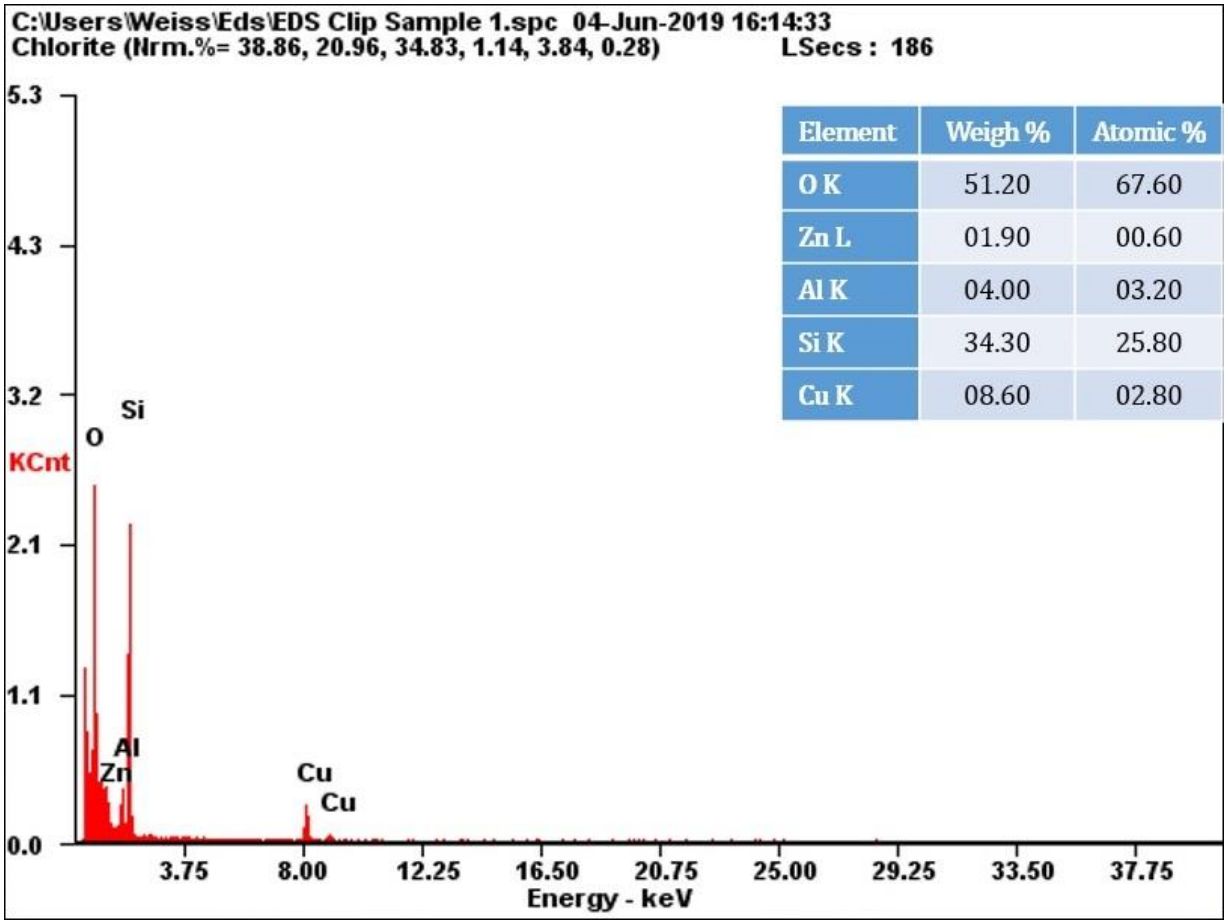

Graph 3.4.1

Hitachi H-9500 HRTEM EDX Microanalysis Report
of Clinoptilolite over Copper/Lacy Carbon TEM Grid

3.5 Hitachi H-9500 HRTEM Images

The images of the clinoptilolite taken with the Hitachi H-9500 High Resolution Transmission Electron Microscope are presented in this section. As previously stated, these images were taken from the same TEM grid that the EDX chemical analysis was performed on. This helps to provide confidence that the elemental and structural

characterization were performed on the same sample material. The setup is an improvement over the SEM's setup where there was one substrate for imaging and another for the EDX chemical analysis.

Unlike the scanning electron microscopes, there were no complications due to charging due to the nature of how TEM's work. This allowed for images with greater magnification to be produced. The HRTEM's magnification capabilities are five-fold to that of the SEM's; the HRTEM will magnify a sample up to x1.5 million while the Hitachi S-4800 FESEM's maximum magnification was x300k.

Figure 3.5.1 shows the TEM grid's carbon mesh; this carbon mesh sits on top of the copper grid and its purpose is to hold up the sample. The object in this image was originally mistaken for the sample until Dr. Jiang from the CCMB at UTA pointed out the error. It is shown here as a "control image" to help confirm that the other images shown are of the sample and not of the TEM grid itself. For an image of carbon at x1.5 million magnification, please see Figure 3.7.1.

Figures 3.5.2 and 3.5.3, show the sample laying over the carbon mesh, at increasing magnifications. The exact magnification is unknown in these images, but note the scale on the lower left corner of 200 and 100 nanometers. These images have less detail than the best SEM images taken of the sample and nothing can be determined from them.

In Figure 3.5.4 one can begin to make out different "clumps" of the sample. These could very well be crystals of clinoptilolite, though it is not possible to tell from the image. Please note the scale of 50 nanometers on the lower left hand corner of this image. The magnification here is at the approximate range in which the Hitachi S-4800 FESEM started experiencing problems with charging when imaging the sample; which puts the magnification at approximately x300k. These two images with similar magnification, Figure 3.5.4 and Figure 2.5.8, look very different and it is not because of the distortion on Figure 2.5.8. Figure 3.5.4 looks transparent, similar to an x-ray image of an object, while Figure 2.5.8 shows the surface topography only.

The reason has to do with the fundamental differences in how SEM's and TEM operate. SEM's use low energy Secondary Electron analysis for three-dimensional imaging of topography; Secondary Electrons originate from the topography and there is no transmission of electrons through the sample; hence, why Figure 2.5.8 shows the surface

topography only. In Transmission Electron Microscopy, the electron is transmitted through the sample to obtain the image; hence, it looks similar to an x-ray image.

The following image were taken with the Hitachi H-9500 HRTEM.

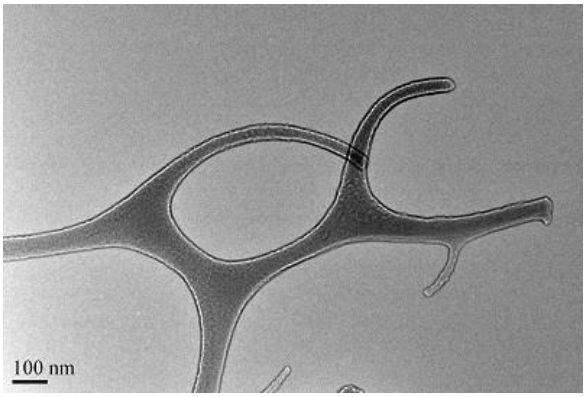

Figure 3.5.1 (above, left side)

Hitachi H-9500 HRTEM
Image of the TEM Grid's Carbon Mesh

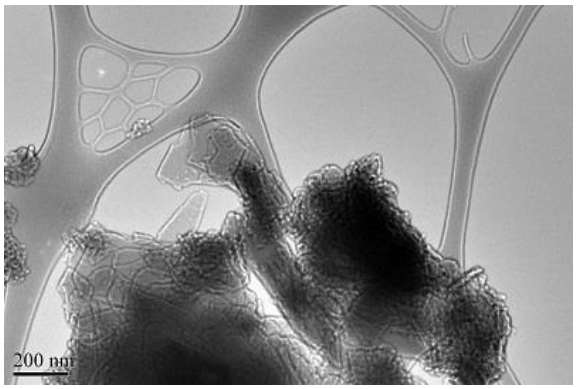

Figure 3.5.2 (above, right side)

Hitachi H-9500 HRTEM Image of
Clinoptilolite over a Carbon Mesh

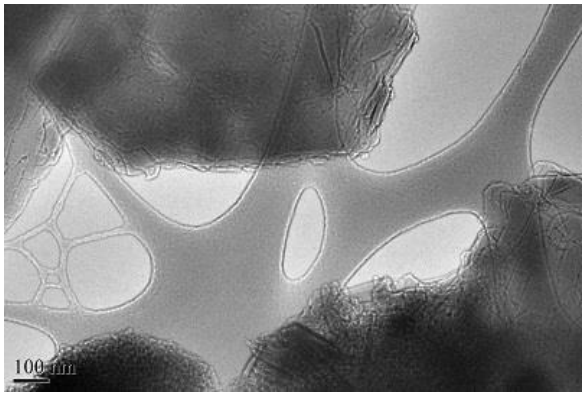

Figure 3.5.3 (left)

Hitachi H-9500 HRTEM Image of
Clinoptilolite over a Carbon Mesh

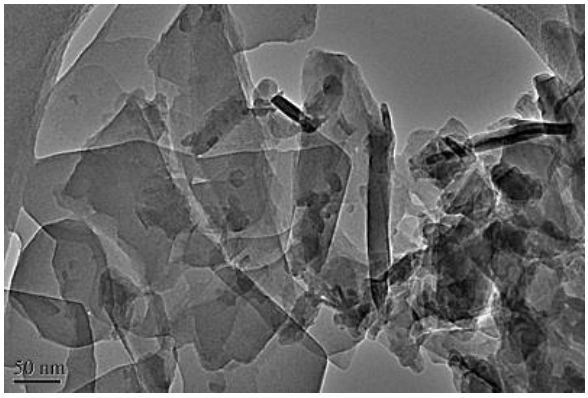

Figure 3.5.4 (right)

Hitachi H-9500 HRTEM
Image of Clinoptilolite "Clumps"

Figures 3.5.5, 3.5.6, 3.5.7, and 3.5.8 were taken at a magnification of x1.5 million, the maximum capability of the Hitachi H-9500 HRTEM. The scale on the lower left hand corner indicates 2 nanometers, which makes the total length of the bar 20 angstroms. This means

the detail and features in these four images is in the angstrom range. TEM images show contrast so a specific type of feature may show up as black in one area of the image while at the same time it may show up as white in another area of the image. The features in these images could be the clinoptilolite holes or they could be another face of the lattice structure. It is not possible to tell without further analysis. The uniform and organized patterns suggest these are definitely crystals of the sample.

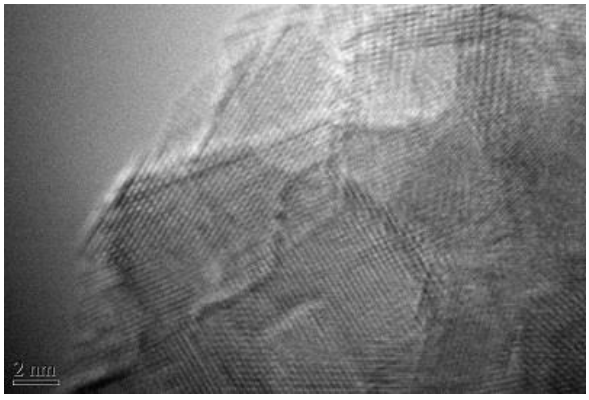

Figure 3.5.5 (above, left side)

Hitachi H-9500 HRTEM Image of Clinoptilolite at x$1.5(10^6)$ Magnification

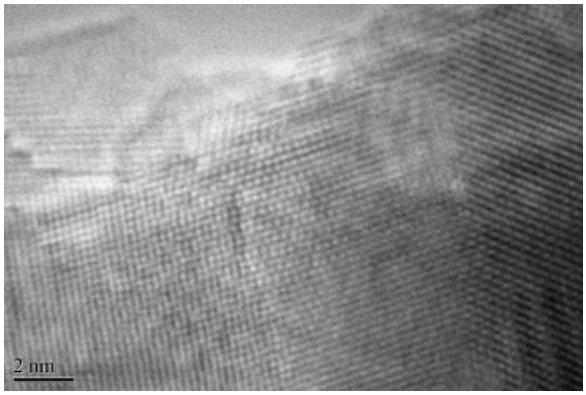

Figure 3.5.6 (above, right side)

Hitachi H-9500 HRTEM Image of Clinoptilolite at x$1.5(10^6)$ Magnification

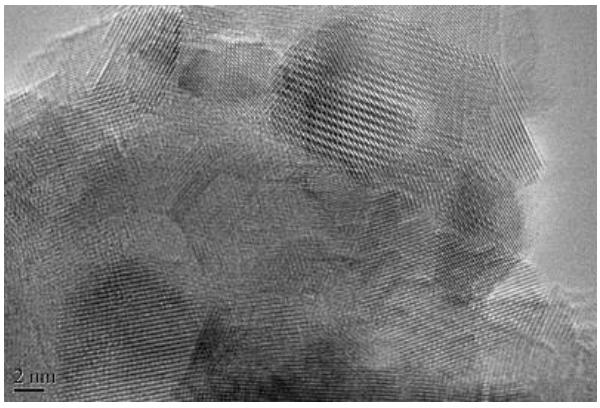

Figure 3.5.7 (left)

Hitachi H-9500 HRTEM Image of Clinoptilolite at x$1.5(10^6)$ Magnification

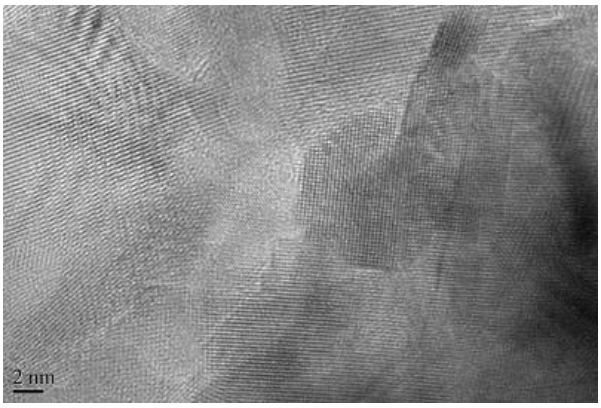

Figure 3.5.8 (right)

Hitachi H-9500 HRTEM Image of Clinoptilolite at x$1.5(10^6)$ Magnification

Figure 3.5.9 "Image Number 26"
Hitachi H-9500 HRTEM Image of Clinoptilolite
over Copper/Lacy Carbon TEM Grid at x750k Magnification

Figure 3.5.9 was designated “Image Number 26” as it was the 26th image taken the day the HRTEM was used. The image is magnified to approximately x750k and it was one of the best images produced by the HRTEM; hence the reason it was made to fit the entire page. The image demonstrates a two dimensional image of a three dimensional topography. This is possible, as the image shows, by overlaying transparent clinoptilolite crystals right on top of one another. Like in the previous images, Figures 3.5.5, 3.5.6, 3.5.7, and 3.5.8, all the features in this image is in the angstrom range at this scale. Also like the previous images, it is not known yet what this features are or what face of the clinoptilolite crystal structure is visible. Further analysis is needed to determine this and it is the focus of the next three sections, Sections 3.6, 3.7 and 3.8.

3.6 Fast Fourier Transform Images

For the Fast Fourier Transform (FFT) analysis, Figure 3.5.9 was used as it was one of the best images produced out of the series. Figure 3.6.1 shows the top right corner of the image in Figure 3.5.9 and are both magnified to x750k. Figure 3.6.1 shows the best area of the image and has been enlarged for clarity; the scale on both of the images read 5 nanometers. The areas chosen for the FFT analysis lie along the edge of the sample where overlap with another crystal structure is at a minimal.

The FFT images obtained using the Hitachi H-9500 HRTEM are shown in Figures 3.6.2, 3.6.3, and 3.6.4. The FFT images were taken of the general area shown in Figure 3.6.1. As the FFT images proved to be difficult to interpret in part due to noise issues, the decision was made to use the real space images for structural analysis as described in the following section.

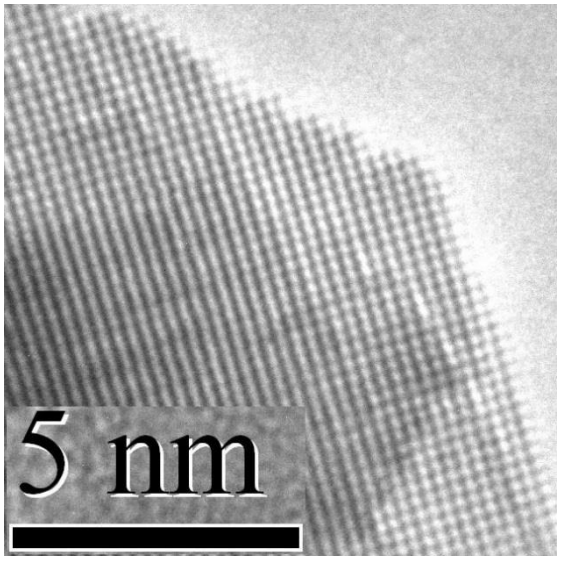

Figure 3.6.1 (above, left side)

Hitachi H-9500 HRTEM Image of Clinoptilolite Crystal Structures Magnified to x750k (unknown plane)

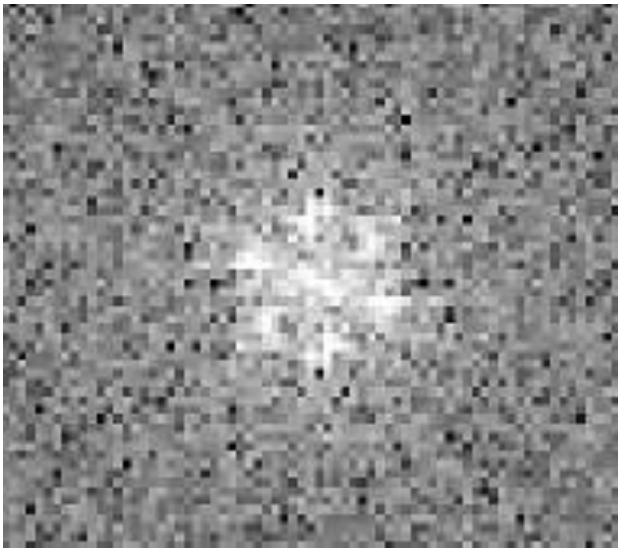

Figure 3.6.2 (above, right side)

Hitachi H-9500 HRTEM FFT Image of Clinoptilolite Crystal (first attempt)

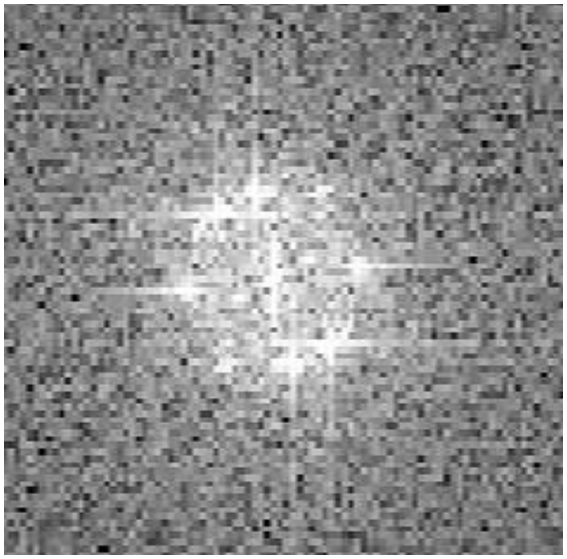

Figure 3.6.3 (left)

Hitachi H-9500 HRTEM FFT Image of Clinoptilolite Crystal (second attempt)

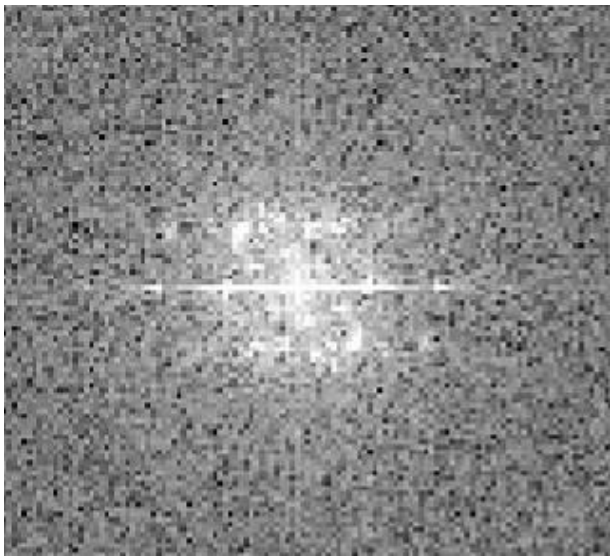

Figure 3.6.4 (right)

Hitachi H-9500 HRTEM FFT Image of Clinoptilolite Crystal (third attempt)

3.7 Method for Counting Atom Spacing

Since the Fast Fourier Transform analysis proved to be inconclusive, an alternate method was used to identify the clinoptilolite lattice structure. This method involves taking measurements of uniform patterns within one of the high resolution images produced by the Hitachi H-9500 HRTEM. These measurements should match known lengths of the clinoptilolite lattice structure. As a test, the method was tried on carbon (C), which has a simpler lattice structure than clinoptilolite.

First, a scale was obtained using a HRTEM image obtained from graphite Figure 3.7.1. This image has a pixel count of 4008 x 2672. Several images were taken but this particular image offered the best quality and greatest magnification, x1.5 million. The scale on the lower left corner for this image reads two nanometers, which is 20 angstroms. Then, a count is made of the pixels that lay across the scale's bar and a calculation is made of pixels per angstrom. **For the image mentioned that calculation came out to be 21.5 pixels per angstrom.**

Figures 3.7.2 and 3.7.3 are a magnified section of the top right hand corner of Figure 3.7.1 and are identical; save for two blue lines on Figure 3.7.3. The blue lines indicate where the measurements were taken; across seven dark spacings instead of one to reduce error in the measurements. The term "spacing" is used out lack of a better term as the contrast between light and dark regions most likely indicate columns of atoms and not single atoms.

After a pixel count is made a bond length was determined. The vertical spacing length is calculated to be approximately 2.69 angstroms and the horizontal spacing length is approximately 2.73 angstroms. That is an average of 2.71 angstroms from the center of each dark circle to the next. Unfortunately the measured length of 2.71 angstroms does not match any of the known bond lengths in hexagonal graphite. This suggests that additional methods of calibration may be necessary.

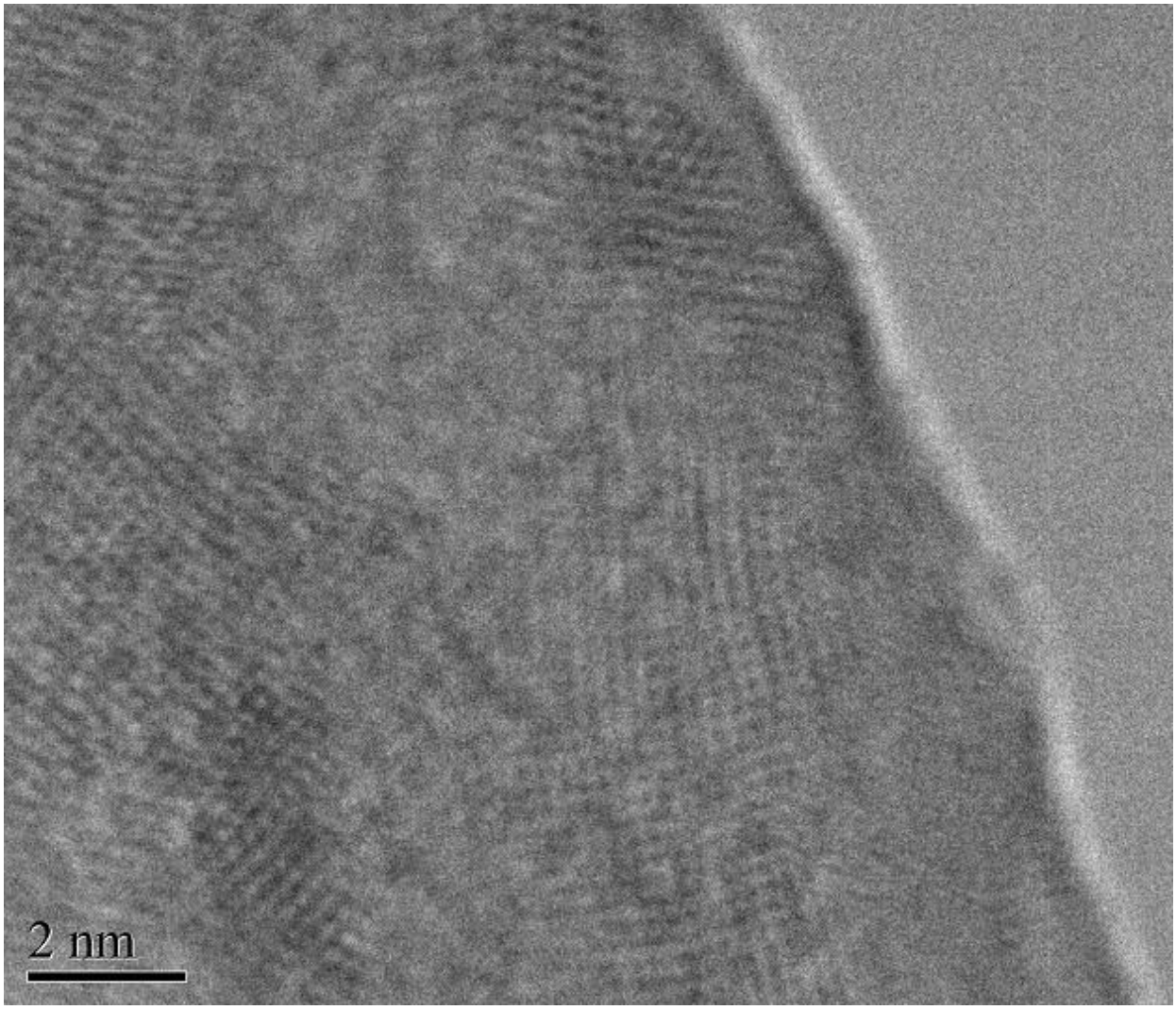

Figure 3.7.1

Hitachi H-9500 HRTEM Image of Graphite
on a Copper/Lacy Carbon TEM grid at X1.5 million magnification
(grid not shown)

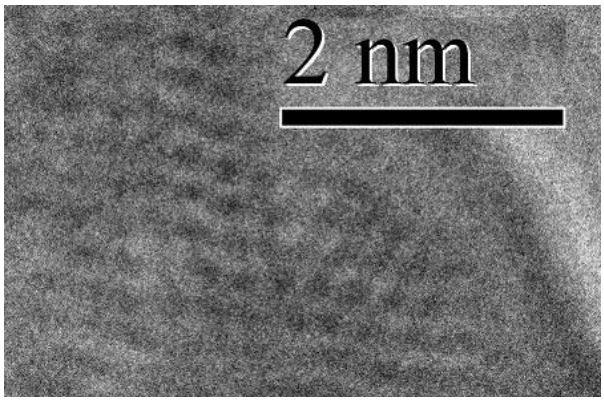

Figure 3.7.2 (left)

Close up of Top Center of Figure 3.7.1

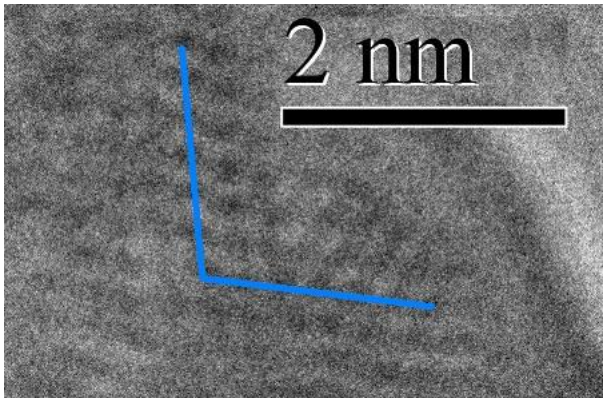

Figure 3.7.3 (right)

Close up of Top Center of Figure 3.7.1

3.8 Identifying the Clinoptilolite Crystal

Figure 3.5.9 shows is magnified to approximately x750k and it was one of the best images obtained in our studies using the HRTEM. The scale is not visible as it was cropped off the picture but it reads 5 nanometers [50 angstroms (Å)]. The pixel count of the image is 4008 x 2672 and the **calculations came out to be approximately 6.76 pixels per angstrom.**

Figures 3.8.1 and 3.8.2 are a magnified section of the top of Figure 3.5.9 and are identical; save for two blue lines on Figure 3.8.2. The blue lines indicate where the measurements were taken; across several white spacings instead of one to reduce error in the measurements. A horizontal and vertical measurement are taken for better thoroughness and accuracy. The vertical spacing length is calculated to be approximately 2.34 Å and the horizontal spacing length is approximately 2.36 Å. **That is an average of 2.35 angstroms from the center of each white circle to the next.** The clinoptilolite lattice structure is very complex and, both, the pattern and this calculation is hard are match with any properties of its lattice structure.

A list of was obtained from the IZA-SC, 2017 database. Table 3.8.1 contains the results of some of the lattice planes for whom the plane spacing was calculated. **The closest match was plane 2 1 2 with a lattice space distance of approximately 2.64 Å; by comparison, the measured distance lattice spacing was 2.35 Å.**

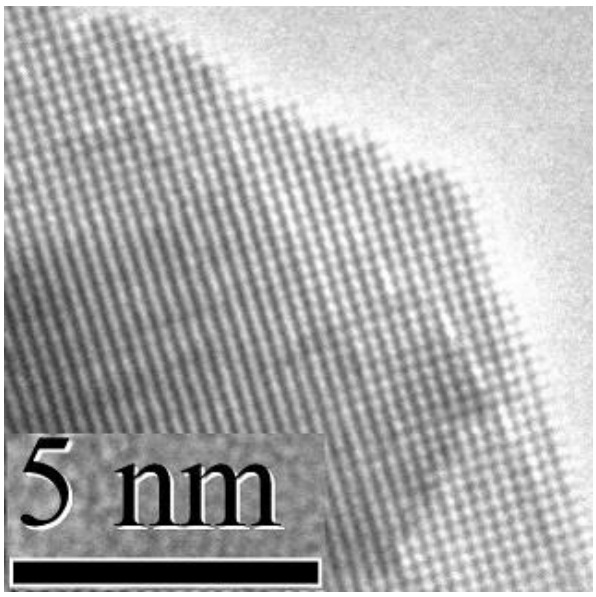

Figure 3.8.1 (left)

Close-Up of Top of Figure 3.5.9
Clinoptilolite at x750k Magnification

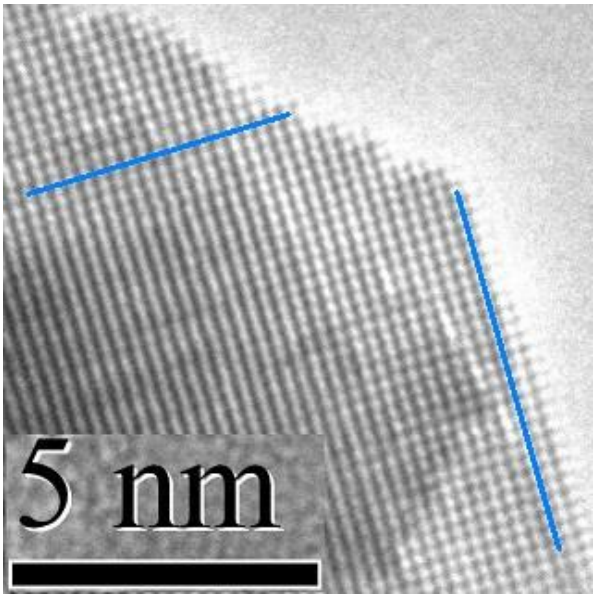

Figure 3.8.2 (right)

Close-Up of Top of Figure 3.5.9
Clinoptilolite at x750k Magnification

Table 3.8.1
Clinoptilolite Crystal Planes and Their Corresponding Lattice Plane Spacing

Planes			Plane Spacing
h	k	l	d (in Angstroms)
1	0	0	15.82006
0	1	0	17.911
0	0	1	6.634537
1	1	0	11.85715
1	0	1	5.33103
0	1	1	6.221435
1	1	1	5.109507
2	2	1	3.831594
2	1	2	2.636479
1	2	2	2.836571

CHAPTER FOUR

Estimates Useful in the Design of Positron Beam Based Experiments on the Clinoptilolite Zeolite

4.1 Introduction

Dr. Alexander Weiss' research group, at the University of Texas at Arlington (UTA), focuses on the study of surfaces, or condensed matter, using the anti-matter beam. More specifically, surfaces are probed using a special type of Electron Auger Spectroscopy (EAS), which is called Positron Annihilation induced Auger Electron Spectroscopy (PAES). In PAES, chemical information from the top atomic layers of the surface is obtained through the analysis of an electron's energy. These electrons, which are emitted from the surface, become ejected from the atom and into the vacuum as a result of the annihilation of core electrons bound in the surface state (Weiss *et al*, 1988). The method of using positrons to induce Auger transitions was first developed here at UTA by Dr. Weiss and his research team in 1987 (Xie, 2002).

As of 2020, there are two anti-matter beams at the University of Texas at Arlington. One of them resides in the Science Hall basement while the other resides in the third floor of the Chemistry and Physics Building (CPB). Both of the beam lines use a Time-of-Flight (ToF) PAES system to collect information. It is the hope of the research group to improve these materials by means of these studies.

4.2 What is a Positron?

The positron is the anti-matter equivalent of the electron. The positron and the electron are the lightest leptons and are a believed to be stable in vacuum, with a lifetime against decay greater than 10^{28} years. However, the two particles can annihilate each other in an event in which both particles disappear and gamma rays are emitted. These high energy photons carry off the energy associated with total energy, including the energy

associated with the rest mass, of the two particles at the time of annihilation. More specifically, when positrons are injected into condensed matter at energies that are small compared to their rest mass energy of 511 keV, annihilation will take place on a time scale of order 10^{-10} seconds; the result will be the emission of 2 gamma rays with an energy of close to 511keV each (Schultz and Lynn 1988).

Positrons can be created by either radioactive decay or by pair production. Pair production is when a gamma ray interacts with matter, giving its momentum to a nearby nucleus causing it to be excited. The process gives off a positron and an electron; some consider pair production the reverse process of positron-electron annihilation. Positron emission can also be achieved through Beta+ decay, which is a type of radioactive decay. It is this later process that is used in the UTA positron beams to attain these anti-matter particles.

4.3 Positron Interactions with Matter

Logic suggests, upon interaction with matter, the first possible type of interaction is that the positron will backscatter off the surface. In the energy range of 345 keV through a few MeV, however, bremsstrahlung is the primary mechanism for a positron's initial loss of speed (Schultz and Lynn, 1988). The term bremsstrahlung can be translated as "breaking radiation" from German. It is when a photon is produced by the deceleration of a charged particle as it interacts with the screened Coulomb of a nucleus or one of its electrons.

For energies in the range of 100 keV through 345 keV, Mott scattering is the primary reason for a positron's energy loss (Schultz and Lynn, 1988). Mott scattering is also known as spin-coupling inelastic Coulomb scattering and it is the separation of the two spin states, 1/2 and -1/2, in a beam of positrons or electrons. The separation occurs when the beam interacts with the electric fields of atoms. Schultz and Lynn go on to suggest that channeling may also play a key role in a positron's deceleration at this stage. Channeling occurs when a beam of positrons, or electrons, interact with the crystal structure of a given material. With the atoms of a material having even spacing between them, the scattering effect of a positron, or electron, beam becomes collective (Sorensen and Uggerhoj, 1989);

meaning the charged particles scatter in “streams” rather than single particles being redirected in random directions.

The next range of energies in which positrons decelerate is from 100keV down to a few tens of electron volts (Perkins and Carbotte, 1970). The deceleration mechanism consists of the excitation of core and valence electrons (Adesida *et al.*, 1980). This happens as the positron interacts with electrons, given off its energy and exciting the electron.

At still lower energies, the type of interactions that occur are entirely dependent on the type of solid, such as metals, semiconductors, ionic solids, and insulators (Schultz and Lynn, 1988). Insulators, which is the type of material that the clinoptilolite is, have larger band gap than semiconductors and ionic solids.

A positron incident, at higher energies, can lose enough energy through inelastic processes to achieve a level comparable to thermal energies before they annihilate; this process is termed thermalization (Kubica and Stewart, 1975). The larger band gap in wide band gap insulators causes the thermalization time of a positron to increase in comparison to metals and typical semiconductors (Gullikson and Mills, 1986). Positron thermalization in insulators involve the formation of positronium and there is debate as to whether full thermalization before annihilation occurs (Schultz and Lynn, 1988). After stopping, the diffusion length will be about 10 to 20 nanometers and its lifetime will be in the hundredths of pico-seconds (Weiss *et al*, 1988).

4.4 Overview of the Positron Beam

The positrons for the UTA positron beam system are obtained by moderating the radiation emitted from encapsulated sodium-22; this source emits positrons as a result of Beta+ decay. Radiation exposure is minimized by encasing the source using lead and tungsten shielding. A fraction of the positrons emitted from the source are slowed using a moderator and then guided through a series of electro-magnets. In the positron beam in CPB, additional small electro-magnets were mounted so as to contribute a magnetic field component at right angles to the beam axis; these fields are used as an energy filter. Positrons having too much, or too little, energy will collide with a barricade while the positrons with the desired energy are allowed to pass.

Once the positrons are energy selected, they are guided by the axial magnetic field through a coaxial metal tube, which is referred to as the ToF tube. The ToF tube may be biased with respect to the grounded beam transport tube. After passing through the ToF tube, the positrons collide with the sample in the sample chamber.

Positrons impinging on the surface with energies less than 1 keV have a high probability of becoming trapped in a surface state; the surface state is localized just outside the surface of the sample and it is where positrons will typically annihilate with electrons. The annihilation of an electron with a positron can result in a hole in a core energy level accompanied by the production of two 511 keV gamma rays. If an electron with a higher energy level drops to the lower energy state and fills the hole then a couple of different other processes can occur. One possibility is that the extra energy is given off as an X-ray photon. The second is that the energy is transferred to another electron thereby expelling it from the atom and into the vacuum; a process known as an Auger transition. In the UTA ToF PAES systems, the energy of the electrons is determined by measuring the time between the detection of a 511 keV gamma ray and the positron-induced electron. (Weiss *et al*, 1988)

The current UTA position beam systems do not allow samples to be easily exchanged. The sample exchange process can take up to a day, assuming nothing else breaks. For comparison, changing the sample in an electron microscope can take no more than 15 minutes; also, assuming nothing else breaks.

A picture of the UTA positron beam system housed in the Science Hall basement is shown in Figure 4.4.1. The two large copper coils at right encircle the lead shielding enclosing the 22Na source. The large coils together with the smaller metal squares are the electro-magnets, or the magnetic lenses of the instrument. The larger metal squares surround the time-of-flight tube. Lastly, the foil surrounding the back part of the instrument encases the sample chamber. The “high voltage” warning signs are placed near parts of the beam where high voltages may be encountered in order to remind lab personnel to exercise extreme caution in these areas.

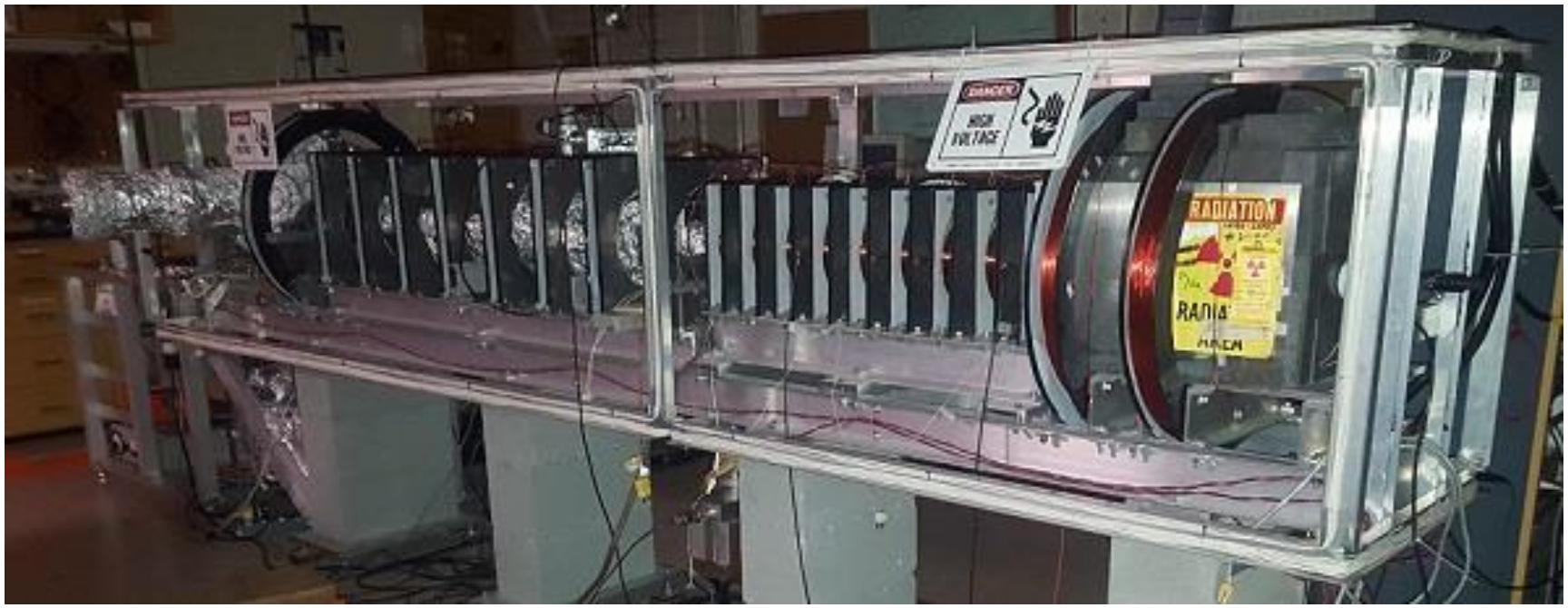

Figure 4.4.1

Science Hall Anti-Matter Beam Line at the University of Texas at Arlington

4.5 Estimates of Positron Implantation Profiles in Clinoptilolite Zeolite

In this section, an estimate of the positrons' implantation distribution into clinoptilolite, after a time corresponding to the thermalization time, will be presented. This distribution is termed the positron implantation profile and it will be used in later calculations; the calculations will ultimately estimate the fraction of positrons that diffuse to and become trapped at the internal surfaces of this zeolite.

Previous studies by Schultz and Lynn have shown that a parameterized function, known as the Makhovian profile, may be used to approximate the distributions of particles; more specifically, the thermalized positrons resulting from implantation using a mono-energetic beam. The parameters are material dependent and are typically found by fitting to Monte Carlo calculations. The calculations for the profile are density dependent and units of grams per cubic centimeter must be used. Since the clinoptilolite crystal is not consistent throughout, an attempt is made to approximate the implantation profile by calculating the Makhovian profile for two densities. The first density is for silicon dioxide (SiO_2), which has a density of 2.65 $g/cm.^3$, and the second density for aluminum oxide (Al_2O_3), which has a density of 4.00 $g/cm.^3$ (Dryzek, 2019). These are known as silica and alumina, respectively.

The first step in the determination of the Makhovian profile is to estimate the parameter, $\boldsymbol{z_0}$, corresponding to the mean implantation depth. Equation 1 relates the incident energy, **E**, to a specific depth, $\boldsymbol{z_0}$, for a given density, $\boldsymbol{\rho}$. The energy calculation, in terms of a specific depth, is needed because the second part of this equation, Equation 5, does not use an energy variable. Equation 1 relates the two so that a final distribution can be calculated. For the purposes of this study, one equation could simply be plugged into the other; although it will be shown as intended on this paper. The following equation relates the incident energy of a mono-energetic beam to its corresponding depth (Van Petegem *et al*, 2004):

$$\boldsymbol{z_0 = \frac{\alpha E^n}{\rho \Gamma\left(\frac{m+1}{m}\right)}} \qquad \textbf{(1)}$$

In this expression, Equation 1, **Γ** is the gamma function and **m**, **n**, and $\boldsymbol{\alpha}$, are parameters for values that differ depending on the material. These values may also differ slightly depending on the source. As an example, on Table 3.4.1, a summary of all the parameters is given as reported by Vehanen *et al*.

Table 4.5.1 Makhov Distribution Variables and Parameters (Vehanen *et al*, 1987)	
z_0: **penetration depth**	$\alpha = 4.0 \pm 0.3\ \mu g\ (cm.)^{-2}\ (keV)^{-1.62}$
ρ: **density**	$m = 2.0 \pm 0.1$
Γ: gamma function	$n = 1.62 \pm 0.05$
$E = mean\ incident\ energy\ in\ kilo\ electron - Volts$	

On Table 4.5.2, the parameters obtained by Dryzek and Horodek from the Monte Carlo simulations, using the GEANT 4 code, are listed; these are used because parameters specific to clinoptilolite are not available. The values for this paper were chosen for the calculations because the list of available parameters and materials more closely coincide with the clinoptilolite chemical makeup. Note that there are some difference in the **m**, **n**, and $\boldsymbol{\alpha}$ values from the Vehanen *et al* values.

Table 4.5.2 Makhov Distribution Variables and Parameters Used (Dryzek and Horodek, 2008)	
Silicon Dioxide (SiO_2)	Aluminum Oxide (Al_2O_3)
$\alpha = 2.32\ \mu g\ (cm)^{-2}\ (keV)^{-n}$ $m = 2.19$ $n = 1.774$ $\rho = 2.65\ \frac{gr.}{(cm)^3}$	$\alpha = 2.38\ \mu g\ (cm)^{-2}\ (keV)^{-n}$ $m = 2.21$ $n = 1.773$ $\rho = 4.00\ \frac{gr.}{(cm)^3}$

The gamma functions can be calculated as:

$$\Gamma\left(\frac{m+1}{m}\right) = \Gamma\left(\frac{m}{m} + \frac{1}{m}\right) = \Gamma\left(1 + \frac{1}{m}\right) = \left(1 + \frac{1}{m} - 1\right)! = \left(\frac{1}{m}\right)! \qquad (2)$$

Using m = 2.19 for the silica value in Equation 2 gives:

$$\left(\frac{1}{m}\right)! \Rightarrow \left(\frac{1}{2.19}\right)! \approx (0.456621)! \approx 0.885614$$

Using m = 2.21 for the alumina value in Equation 2 gives:

$$\left(\frac{1}{m}\right)! \Rightarrow \left(\frac{1}{2.21}\right)! \approx (0.452489)! \approx 0.885639$$

Now, a specific and density-dependent depth that corresponds to a given incident energy can be calculated. Plugging in the values and adjusting the equation for microns, simply because microns will make calculations easier at the end, the silica equation can be reduced to:

$$z_0 = \frac{\alpha E^n}{\rho\Gamma\left(\frac{m+1}{m}\right)} = \frac{2.32(10^{-6})\frac{gr.}{cm.^2 \cdot keV^{1.774}} \cdot E^{1.774}}{2.65\,\frac{gr.}{(cm)^3}(0.885614)}\left(\frac{10^4\,\mu m.}{1\,cm.}\right) \Rightarrow$$

$$\boxed{z_0 \approx 9.88548 \cdot 10^{-3}\ microns\left(\frac{E^{1.774}}{keV^{1.774}}\right)} \qquad (3)$$

Where **E** is the positron energy in kilo-electron-Volts.

Likewise, the alumina equation for a specific and density-dependent depth that corresponds to a given incident energy can be reduced to:

$$z_0 = \frac{\alpha E^n}{\rho \Gamma\left(\frac{m+1}{m}\right)} = \frac{2.38(10^{-6})\frac{gr.}{cm.^2 \cdot keV^{1.773}} \cdot E^{1.773}}{4.00\ \frac{gr.}{(cm)^3}(0.885639)}\left(\frac{10^4\ \mu m.}{1\ cm.}\right) \Rightarrow$$

$$\boxed{z_0 \approx 6.71831 \cdot 10^{-3}\ microns\left(\frac{E^{1.773}}{keV^{1.773}}\right)} \qquad (4)$$

Now, in Graph 4.5.1, both equations are graphed for multiple values of the implantation energy. The values of 1 keV through 20 keV are used; these values correspond to energies that are achievable by the UTA positron beam systems. The silica energy-to-depth-relation values are given by the blue line and the alumina energy-to-depth-relation values results are given by the orange line. The precise values for the graph are given in Table 4.5.3. **One should note that these are not positron penetration depth probability values;** those are calculated in the next section.

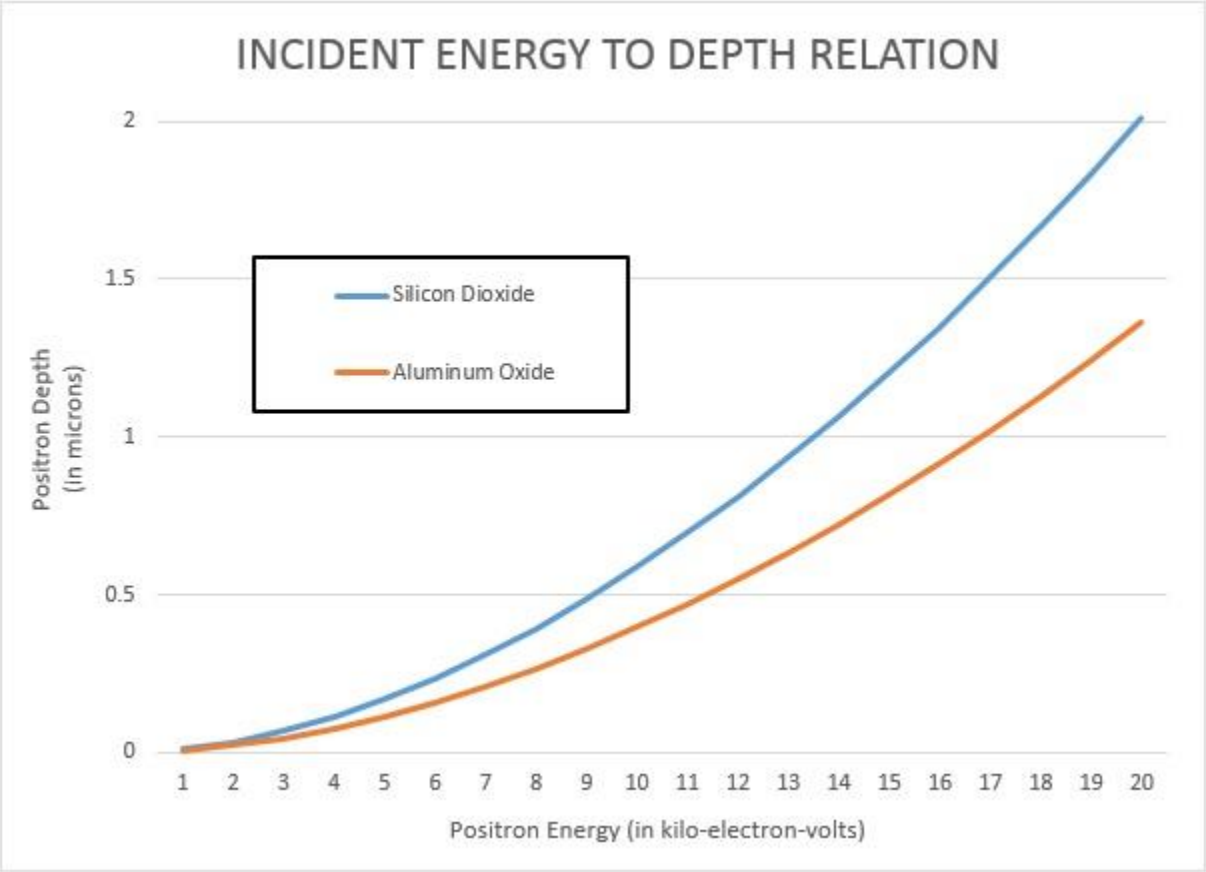

Graph 4.5.1

Calculated corresponding positron depths (in microns)
according to their energy (in kilo electron-Volts).

Table 4.5.3 Energy to Depth Relation Values According to Incident Energy		
Energy (in kilo electron-Volts)	Silicon Dioxide (SiO_2) (in microns)	Aluminum Oxide (Al_2O_3) (in microns)
1	0.009885477	0.006718312
2	0.033808419	0.022960765
3	0.069408196	0.04711901
4	0.115625088	0.078471606
5	0.171779146	0.116555828
6	0.237376636	0.161035765
7	0.312033753	0.211650354
8	0.395438808	0.268187617
9	0.487330804	0.330470079
10	0.587486176	0.398345738
11	0.695710047	0.471682111
12	0.811830161	0.550362106
13	0.935692522	0.634281053
14	1.067158154	0.723344498
15	1.206100633	0.817466525
16	1.35240417	0.91656845
17	1.505962087	1.020577789
18	1.666675594	1.129427418
19	1.834452792	1.243054899
20	2.00920784	1.361401915

4.6 The Makhovian Profile

To complete the implantation profile, the second equation for the Makhov distribution, Equation 5, is used. This function is the part of the calculation where the probability of positrons that will annihilate at specific depths is determined. The second equation of the Makhov profile distribution is (Schultz and Lynn, 1988):

$$P(z,E) = \frac{mz^{m-1}}{z_0^m} \cdot exp\left[-\left(\frac{z}{z_0}\right)^m\right] \quad (5)$$

where **P** is the probability, **m** is the parameter discussed in the previous section, z_0 is a value for the energy of the positron in terms of a corresponding depth, and **z** is the variable for depth.

One can see from Table 4.5.3 that, for silica, the positron energy of 20 keV corresponds to a penetration depth of 2.009 microns. Therefore, for z_0, the value of 2.009 microns is used instead of 20 keV, as seen in the corresponding Equation 6. Similarly, Equations 7, 8, 9, and 10 contain the appropriate z_0 silica Makhovian profile values for energies 15 keV, 10 keV, 5 keV, and 1 keV respectively. Equations 11, 12, 13, 14, and 15 contain the appropriate z_0 alumina Makhovian profile values for energies 20 keV, 15 keV, 10 keV, 5 keV, and 1 keV also respectively. The parameter **m** was kept unchanged for each compound; 1.9 for the silica values and 2.1 for the alumina values.

Graphing these equations gives the Makhovian profile for the silica values, Graph 4.6.1, and the alumina values, Graph 4.6.2. These graphs show the incident energy values, 20 keV, 15 keV, 10 keV, and 5 keV, while omitting the 1 keV value. The 20 keV, 15 keV, 10 keV, and 5 keV curves graph well together because they are all within one order of magnitude away from each other; therefore the information is discernable. The 1 keV curve had to be graphed separately because the 1 keV depth to energy relations values are 2 orders of magnitude different than any of the other energy relation values. This method was implemented to better be able to present the information, as graphing all the values on one graph causes the information to be indiscernible. Therefore, in Graph 4.6.3, the 1 keV values for silica and alumina are graphed together.

The Makhovian profiles provide an idea of how deep a positron will penetrate at a given incident energy. When appropriately normalized, the integral of the profile between two values, z_1, and z_2, will correspond to the probability of finding the positron somewhere in the range $z_1 < z < z_2$; thus the area from under each curve integrated from 0 to ∞, should equal unity.

One can see, on Graph 4.6.1, that for silica, a positron with an incident energy of 5 keV has a next to zero probability of penetrating deeper than half a micron. Also, it may be seen from Graph 4.6.2 that, for alumina, positrons with an incident energy of 20 keV will mostly penetrate well under half a micron and a few will even penetrate as far as 2.5 microns. **This information is necessary to determine where the positron interactions are taking place.**

One has to remember that **these values are very conservative**. Silica has a density of 2.65 gr/cm^3 and alumina has a density of 4.00 gr/cm^3. However, clinoptilolite is not only a caged structure but it is also very porous at the macro level; the mineral's crystals are inconsistent, held together in "clumps" by Van der Waals forces, and there is a lot of space within the material. **The clinoptilolite's bulk density is between 0.72083 and 0.86500 gr/cm^3 and the manufacturer's quoted specific gravity is 1.89 gr/cm^3.** Unfortunately, there are no Makhovian parameters available for clinoptilolite; ergo, an estimate is made using the parameters for silica and alumina. There are other factors that will ultimately determine the penetration depth and those factors are discussed in the conclusions in Chapter 5.

Graphing Equations 6 through 15 give the **Makhovian Profiles** shown in Graphs 4.6.1, 4.6.2, and 4.6.3 for the incident energies of 20 keV, 15 keV, 10 keV, 5 keV, and 1 keV:

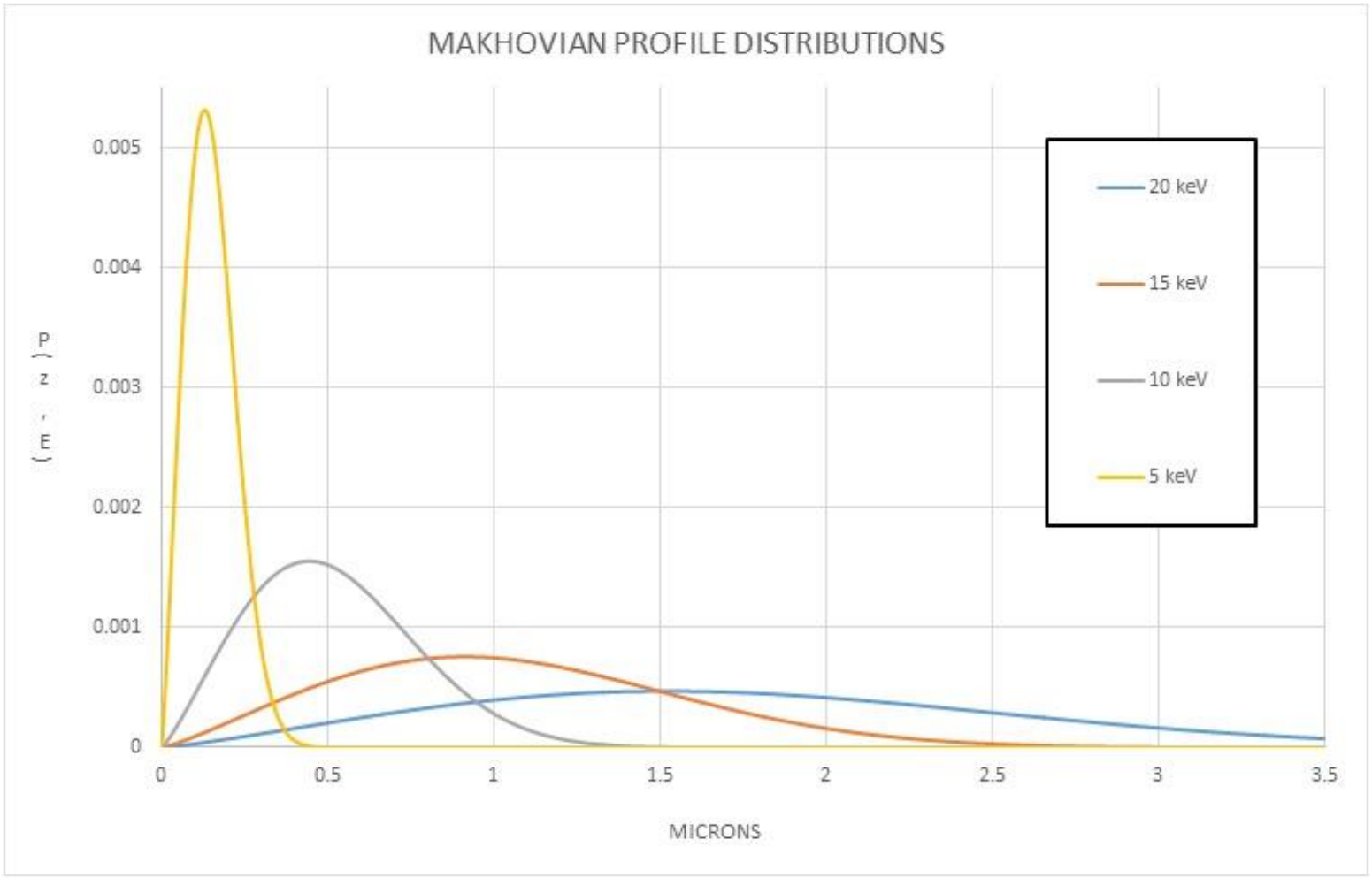

Graph 4.6.1

Silicon Dioxide (SiO_2) Makhovian Profile Distributions for the Incident Energies: 20 keV, 15 keV, 10 keV, and 5 keV.

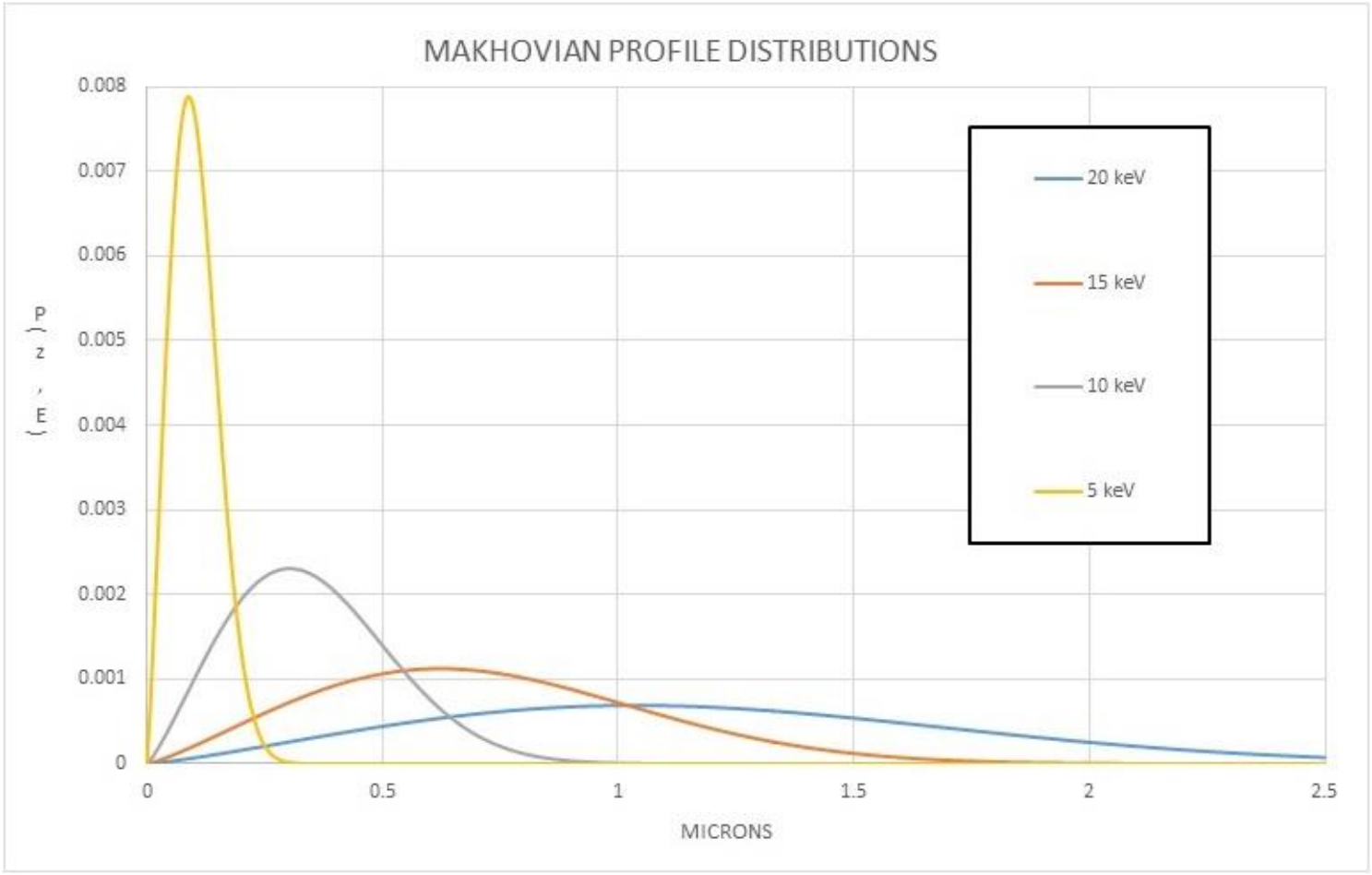

Graph 4.6.2

Aluminum Oxide (Al_2O_3) Makhovian Profile Distributions for the Incident Energies:
20 keV, 15 keV, 10 keV, and 5 keV.

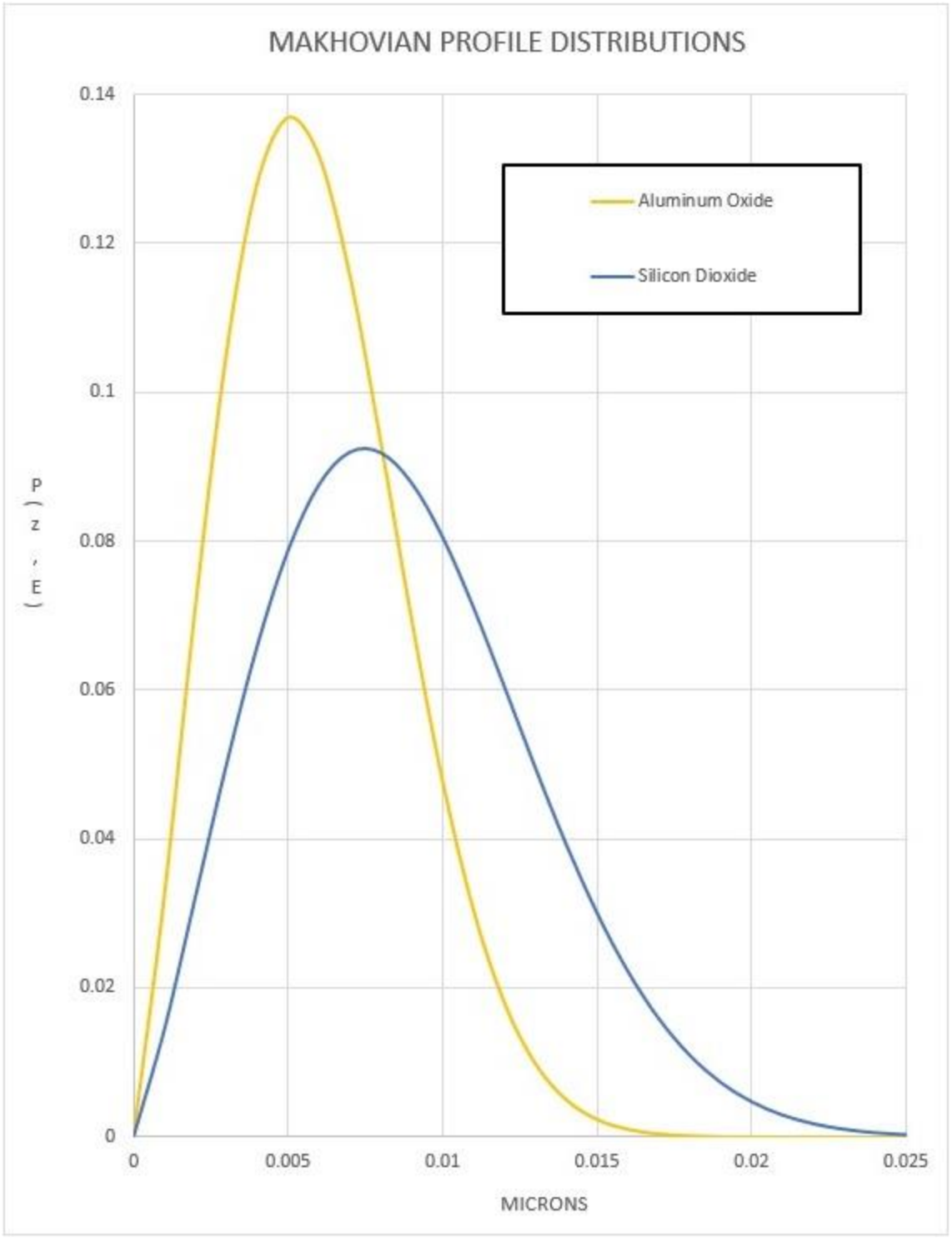

Graph 4.6.3

Silicon Dioxide (SiO_2) and Aluminum Oxide (Al_2O_3) Makhovian Profile Distributions for the Incident Energy of 1 keV.

Silicon Dioxide (SiO_2) Makhovian Profile Equations

The equation for **20 keV** is:

$$\boldsymbol{P(z,E) = \frac{2.19 \cdot z^{1.9}}{[2.009\,(10^{-6})m.]^{2.9}} \cdot exp\left[-\left(\frac{z}{2.009\,(10^{-6})m.}\right)^{2.19}\right]} \quad (6)$$

The equation for **15 keV** is:

$$\boldsymbol{P(z,E) = \frac{2.19 \cdot z^{1.9}}{[1.206(10^{-6})m.]^{2.9}} \cdot exp\left[-\left(\frac{z}{1.206(10^{-6})m.}\right)^{2.19}\right]} \quad (7)$$

The equation for **10 keV** is:

$$\boldsymbol{P(z,E) = \frac{2.19 \cdot z^{1.9}}{[0.5875(10^{-6})m.]^{2.9}} \cdot exp\left[-\left(\frac{z}{0.5875(10^{-6})m.}\right)^{2.19}\right]} \quad (8)$$

The equation for **5 keV** is:

$$\boldsymbol{P(z,E) = \frac{2.19 \cdot z^{1.9}}{[0.1718(10^{-6})m.]^{2.9}} \cdot exp\left[-\left(\frac{z}{0.1718(10^{-6})m.}\right)^{2.19}\right]} \quad (9)$$

And finally, the equation for **1 keV** is:

$$\boldsymbol{P(z,E) = \frac{2.19 \cdot z^{1.9}}{[9.885(10^{-9})m.]^{2.9}} \cdot exp\left[-\left(\frac{z}{9.885(10^{-9})m.}\right)^{2.19}\right]} \quad (10)$$

Aluminum Oxide (Al_2O_3) Makhovian Profile Equations

The equation for **20 keV** is:

$$\boldsymbol{P(z,E) = \frac{2.21 \cdot z^{1.21}}{[1.361(10^{-6})m.]^{2.21}} \cdot exp\left[-\left(\frac{z}{1.361(10^{-6})m.}\right)^{2.21}\right]} \quad (11)$$

The equation for **15 keV** is:

$$\boldsymbol{P(z,E) = \frac{2.21 \cdot z^{1.21}}{[0.8174(10^{-6})m.]^{2.21}} \cdot exp\left[-\left(\frac{z}{0.8174(10^{-6})m.}\right)^{2.21}\right]} \quad (12)$$

The equation for **10 keV** is:

$$\boldsymbol{P(z,E) = \frac{2.21 \cdot z^{1.21}}{[0.3983(10^{-6})m.]^{2.21}} \cdot exp\left[-\left(\frac{z}{0.3983(10^{-6})m.}\right)^{2.21}\right]} \quad (13)$$

The equation for **5 keV** for is:

$$\boldsymbol{P(z,E) = \frac{2.21 \cdot z^{1.21}}{[0.1166(10^{-6})m.]^{2.21}} \cdot exp\left[-\left(\frac{z}{0.1166(10^{-6})m.}\right)^{2.21}\right]} \quad (14)$$

And finally, the equation for **1 keV** is:

$$\boldsymbol{P(z,E) = \frac{2.21 \cdot z^{1.21}}{[6.718(10^{-9})m.]^{2.21}} \cdot exp\left[-\left(\frac{z}{6.718(10^{-9})m.}\right)^{2.21}\right]} \quad (15)$$

CHAPTER FIVE

Conclusions

This thesis has reported on research on the clinoptilolite zeolite; the goal of this research was to provide background information to aid in the interpretation of the data obtained using positron beam based spectroscopies. It has been proposed that these spectroscopies could be used to characterize the internal surfaces of the zeolite materials (Weiss *et al.*, 2020). Information was obtained on the zeolite's chemical composition and structure; estimates were made on the depth to which positrons from the UTA positron beam system could be implanted below the zeolites external surface.

A characterization was conducted on the sample obtained from KMI Zeolite using available equipment on campus. The main focus of the study was to obtain an image of the sample, its chemical composition, and measurements of the crystal lattice's dimensions. The chemical composition of the as received clinoptilolite zeolite material, as listed by the manufacturer: $\boldsymbol{Na_3[Al_3Si_{15}O_{36}]12H_2O}$, was confirmed using Energy-dispersive X-ray spectroscopy (EDX/EDS) for chemical analysis, low energy Secondary Electron (SE) analysis for three-dimensional imaging and topography, and Transmission Electron Microscopy (TEM) for two-dimensional imaging at the angstrom level.

The EDX chemical analysis was done with the Hitachi S-3000N VPSEM. It was verified, with this instrument, that the chemical composition of the sample was of the appropriate ratios to be the clinoptilolite mineral. The imaging was initially done the Hitachi S-4800 II FESEM. This instrument was not able to produce an image with enough magnification to discern any crystal features as problems with sample charging materialized. Charging caused interference with the FESEM's instruments and the result were blurry and fuzzy images. An attempt to rectify the problem with a coating of silver was attempted but not much more magnification could be mustered.

The Hitachi H-9500 High-Resolution Transmission Electron Microscope (HRTEM) comes equipped with an EDAX/EDS system, therefore, the chemical composition of the sample was verified a second time with success; the elemental ratios matched that of what

was expected in clinoptilolite. The images taken with this instrument were magnified up to 1.5 million times and detail in the angstrom level was visible. However, the best and clearest image, Image Number 26, was taken at x750k magnification; since it was the best image, it was subjected to Fast Fourier Transform (FFT) analysis using the available instruments of the HRTEM. All three FFT images taken with the HRTEM had no discernable evidence of the sample being clinoptilolite as there are no measurements that can be taken from them; the diffraction pattern was simply too distorted, unclear, and fuzzy.

Using the pixel count on the same high definition image, Image Number 26, which was the subject of the FFT analysis, a pixel to angstrom ratio could be determined; at that point measurements of the features and structure within the image could be taken. **It was determined that the lattice spacing length was an average of 2.35 angstroms.** Then, using the X-Ray Powder Pattern information generated for clinoptilolite, already available online from the Database of Zeolite Structures (IZA-SC, 2017), a match could be made between the dimensions of the crystal lattice taken from Image Number 26 and a specific crystal plane of the clinoptilolite lattice. The closest match was plane 2 1 2 with a lattice space distance of approximately 2.64 angstroms; by comparison, the measured distance lattice spacing was 2.35 angstroms. The results are sufficiently convergent to be called a match.

The information on the structure and chemical content of the zeolite material, detailed in Chapters 1 through 3, were used in calculations detailed in Chapter 4; the calculations aimed at estimating the implantation profile and the mean depth of implantation of positrons as a function of incident positron energy. The details of the calculations used to estimate the penetration depth of positrons implanted into the clinoptilolite zeolite were included.

When predicting what might happen when the sample is exposed to positrons, one has to consider that clinoptilolite has open volumes known to effectively trap positively charged cations. These cavities could behave like defects in a material that has a potential to trap positrons (Dryzek, 2019). It is, therefore, likely that positrons implanted below the surface will not be able to diffuse back to the external surface, as is possible when positrons are implanted within a few thousand angstroms below an annealed metal.

It should be noted that the implantation profiles shown in Graphs 4.6.1, 4.6.2, and 4.6.3 are for homogenous silica and alumina respectively. As a first approximation, it may be assumed that the zeolite material may be thought of as consisting primarily of silica (~67%) with an admixture of alumina (~11%) and other constituents. Thus, it could be assumed that the implantation profile in the zeolite would lie somewhere in between that of silica and alumina. However, the zeolite's specific gravity of 1.89 gm/cc is 30% lower than the density of silica (~2.65 gm/cc); due to the open structure of the zeolite. Given the inverse relationship between density and $\boldsymbol{z_0}$, (see Chapter 4, Equation 1), it might be expected that the peak of the implantation profile at a given energy would occur at a depth up to 40% larger than that of silica.

On the other hand, when estimating the initial implantation profile, it was assumed that the stopping profiles were functions primary of the material density and that the material was homogeneous. However, it is possible that the density modulations, that are associated with the open volumes in the zeolite, might result in enhanced energy loss mechanisms; these could lead to a significant decrease in the mean implantation depth. A positron will encounter increased stopping power associated with the density modulations due to the open zeolite structure. If it is assumed that the effects of the lower average density, associated with the open volume of the zeolite, largely compensates for this enhanced stopping power, then it can be estimated from Graphs 4.6.1 and 4.6.2 that the peak of the implantation profiles will be at ~0.4 microns for a positron beam of 10 keV.

Graph 5.1 shows the mean implantation depth, $\overline{\boldsymbol{z}}$, as a function of the incident positron kinetic energy for clinoptilolite, silica, and alumina; these were obtained using the formula (Dryzek, 2019):

$$\overline{\boldsymbol{z}} = \frac{\boldsymbol{\alpha E^n}}{\boldsymbol{\rho}} \qquad (16)$$

The curves for silica and alumina were produced by using values of $\boldsymbol{\alpha}$ and $\mathbf{n}$ from Dryzek and Horodek, 2008, as listed in Table 4.5.2. The curve for clinoptilolite was produced using values of $\boldsymbol{\alpha}$ and $\mathbf{n}$ obtained by averaging the values for silica and alumina and assuming that $\boldsymbol{\rho = 1.89\ gr/cm^3}$, the specific gravity for clinoptilolite quoted by the manufacturer.

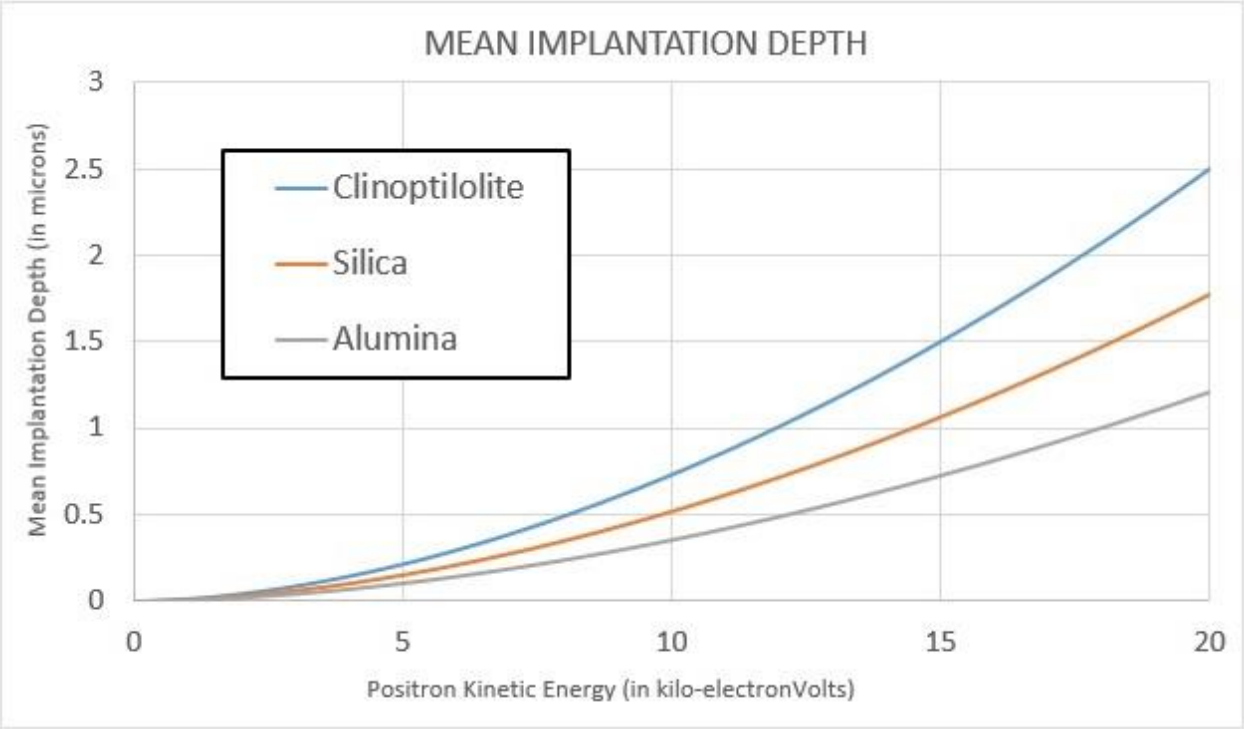

Graph 5.1

The Mean Implantation Depth, $\bar{z}$, as a Function of the Incident Positron Kinetic Energy for the Materials: Clinoptilolite, Silica, and Alumina.

These estimates strongly suggest that the UTA Positron Beam system, which is capable of delivering positrons at energies up to 15 keV, should be more than capable of implanting positrons deep enough to probe the internal surfaces of zeolite materials. Thus, it should be possible to use the UTA positron beam system to conduct experiments to test the sensitivity and utility of positron spectroscopies; this will, in turn, help to probe chemically important properties of the internal surfaces of zeolites.

REFERENCES

Adesida, I., R. Shimizu, and T. E. Everhard, 1980, J. Appl. Phys. 51, 5962.

Advameg, *Zeolites*, Chemistry Explained: Foundations and Applications, 2019 http://www.chemistryexplained.com/

CCMB, "*Instrumentation"*, UTA Characterization Center for Materials and Biology, Accessed 2019. https://ccmb.uta.edu/

Dryzek, J. and P. Horodek, "*GEANT4 Simulation of Slow Positron Beam Implantation Profiles*", Nuclear Instruments and Methods in Phys. Res. B, 266 (2008) 4000-4009

Dryzek, Jerzy. "Positron trapping at defects". Instytut Fizyki Jadrowej. Accessed August of 2019. https://www.ifj.edu.pl/private/jdryzek/page_r15.html

Gullikson, E. M., and A. P. Mills, Jr., 1986, Phys. Rev. Lett. 57, 376.

Hsieh, C. H., Himani Jain, and Efstratios Kamitsos, *Correlation between dielectric constant and chemical structure of sodium silicate glasses*, Journal of Applied Physics, 80. 1704 - 1712. 10.1063/1.363824, September 1996.

IMPS, Is My Pet Safe?, *On Sale But Is It Safe?: LitterMaid Natural Zeolite Litter Box Deodorizer*, Is My Pet Safe: Challenging myths and marketing hype, Accessed August 15, 2019. http://ismypetsafe.com

IZA-SC, Structure Commission of the International Zeolite Association, *Framework Type HEULANDITE*, Database of Zeolite Structures, 2017. http://www.iza-structure.org/databases/

Jiang, Jiechao, *H-9500 High-Resolution TEM Operation Manual*, Characterization Center for Materials and Biology at the University of Texas at Arlington, March 27th, 2009

KMI Zeolite, Mineral Deposit Chemical Analysis, KMI Zeolite, 2018. https://www.kmizeolite.com/

Kubica, P., and A. T. Stewart, *Thermalization of Positrons and Positronium*, Phys. Rev. Lett. 34, 852, April 7, 1975.

Lenntech B. V., *Zeolites: Applications*, Water Treatment Solutions, 1998 https://www.lenntech.com/

Perkins, A., and J. P. Carbotte, 1970, Phys. Rev. B 1, 101.

ResearchGate, *Question: "Can anybody give the details that why hydrogen is not present in EDX SPECTRUM?"*, ResearchGate, August 29th, 2015. https://www.researchgate.net/post/Can_anybody_give_the_details_that_why_hydrogen_is_not_present_in_EDX_SPECTRUM

Schultz, P. J., and K. G. Lynn, *Interaction of positron beams with surfaces, this films, and interfaces*, Reviews of Modern Physics, Vol. 60, No. 3, July 1988

Solyman, Sanaa M., Noha A.K. Aboul-Gheit, Fathia M. Tawfik, M. Sadek, and Hanan A. Ahmed, Performance of ultrasonic – Treated nano-zeolites employed in the preparation of dimethyl ether, Egyptian Journal of Petroleum, 22, 91-99, 2013.

Sorensen, Allan H., and Erik Uggerhoj, *The Channeling of Electrons and Positrons: Charged particles traveling along a crystal's planes of symmetry behave strangely: they interact with sheets or strings of nuclei rather than with single atoms*, Scientific American, Vol 260, No. 6, June 1989.

SPI, "*SPI Supplies Brand TEM Grids G300, 300 Mesh, Copper, 3.05 mm*", Vial of 100, SPI Supplies, Accessed 2019. https://www.2spi.com/item/2030c-xa/

Tedpella, Lacey, Ted Pella, Inc.: Microscopy Products for Science and Industry, Accessed 2019. https://www.tedpella.com/Support_Films_html/

ThermoFisher, *Material Science: "Scanning Electron Microscopy"*, ThermoFisher Scientific, Accessed 2019. https://blog.phenom-world.com/sem-electrons

Touchstone Essentials, Zeolites and Low Level Radiation Exposure, Touchstone Essentials, 2011. https://thegoodinside.com/

Van Petegem, S., *et al*, *Diffusion length of positrons and positronium investigated using a positron beam with longitudinal geometry*, Physical Review B 70, 115410 (2004).

Vehanen, A., K. Saarinen, P. Hautojarvi, and H. Huomo, Phys. Rev. B 35, 4606 (1987).

Weiss, Alex, *et al*, *Elemental Characterization of the Topmost Atomic Layer of Surface Using Doppler Broadening Spectroscopy*, Acta Physica Polonica, 2020. http://przyrbwn.icm.edu.pl/APP/PDF/137/app137z2p01.pdf

Weiss, Alex, *et al*, *Auger-electron emission resulting from the annihilation of core electrons with low energy positrons*, Physical Review Letters, 61.19 1988:2245.

Xie, Shuping, *Positron Annihilation Induced Auger Electron Spectroscopy of Inner Shell Transitions Using the Time-of-Flight Technique* doctoral dissertation, The University of Texas at Arlington, December 2002, UMI Number: 3078654.

[THIS PAGE INTENTIONALLY LEFT BLANK]